ELSEVIER

RESEARCH: Review

Organic materials for rechargeable sodium-ion batteries

Yang Xu [1], Min Zhou [1], Yong Lei *

Institute of Physics and Macro- and Nanotechnologies MacroNano® (IMN & ZIK), Ilmenau University of Technology, Ilmenau 98693, Germany

Rechargeable sodium-ion batteries (SIBs) have attracted great attention for large-scale electric energy storage applications and smart grid owing to the abundance of Na resources and comparable performance with lithium-ion batteries. The use of organic electrode materials enables a sodium storage system with high energy/power density, metal-free, environmental friendliness, flexibility, lightweight, and cost-effectiveness. More importantly, the structural diversity and the ease of functionalizing organic molecules allows straightforward controllability on the redox properties and thus on the battery performances. Despite the development of organic SIBs is still in its infant state, they have drawn dramatically growing attentions and shown great promises throughout research works. In this review, we summarize the research efforts to push forward the electrochemical performance of the organic SIBs. We explore the efforts made on molecular design and electrode design, and the combination of both forms the basis to regulate the electrochemical properties. Moreover, we summarize the strategies for reducing the solubility of the organic electrode materials in light of the importance of this issue. The crucial differences between organic lithium-ion batteries and organic SIBs are presented. Finally, future challenges and opportunities of further developing organic electrode materials are discussed.

Introduction

Electrochemical energy storage (EES) technologies are renewable and environmentally responsible energy storage solutions, and have shown great promise owing to the appealing features such as high round-trip efficiency, long cycle life, low maintenance, and flexible power and energy characteristics to meet different grid functions [1]. Among various EES technologies, lithium-ion batteries (LIBs) are certainly a contender and the last two decades have seen a dramatically increased interest on them through not only the exponential growth of research papers and patents but also their dominance of the market of portable electronics. However, costs and availability of global lithium resources associated with the geographically uneven distribution have created serious concerns with the competitiveness of LIBs. It has been argued that lithium might become the 'new gold' [2]. In this perspective, sodium provides an alternative because of its natural abundance, wide geographical distribution, and similarities with lithium on electrochemistry. Indeed, sodium-ion batteries (SIBs) were studied parallel to LIBs back to the 1980s [3–7] but generally left aside due to the commercial success of LIBs in the 1990s. It was not until a few years ago that room-temperature SIBs came back into research focus (Fig. 1a). Research activities have been rapidly expanding and a large amount of materials have been explored. The development of SIB is now in full swing [8–18].

The majority of SIB materials are typically inorganic. There are rather limited existing recycling strategies for inorganic electrode materials and the strategies are dependent on a large consumption of energy and toxic chemicals [19]. Although Na resources are abundant, such consumption can certainly cause environmental problems and large price fluctuations given the

* *Corresponding author.*
E-mail address: Lei, Y. (yong.lei@tu-ilmenau.de).
[1] These authors contributed equally to this work.

https://doi.org/10.1016/j.mattod.2017.07.005

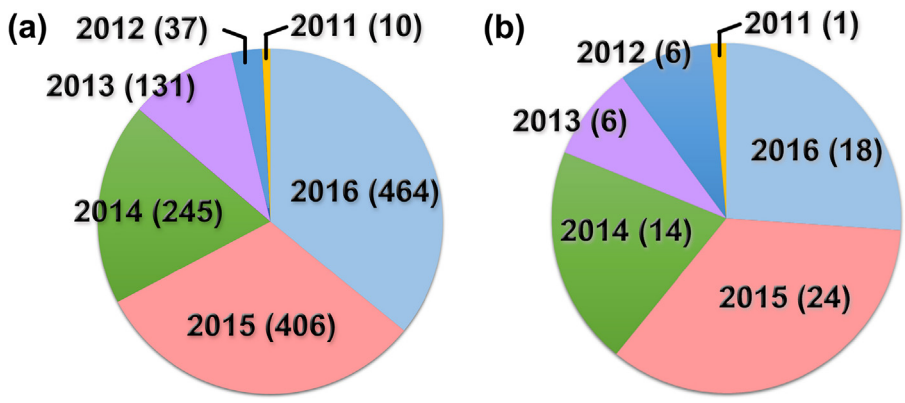

FIG. 1

Pie charts of the scientific papers related to SIB (a) and OSIB (b) published between 2011 and 2016. Data were collected using the ISI Web of Science.

consideration that demand of SIBs may increase once the commercial breakthrough is reached. Organic SIB (OSIB) electrode materials display several inherent advantages over inorganic counterpart. First, organic materials are composed of naturally abundant elements (C, H, O, N, S) and the low atomic weights of the elements give rise to high theoretical gravimetric capacities. Second, organic materials can be harvested from biomass resources with proper design and thermally disposed using low-temperature processes due to the absence of metals, possibly achieving low environmental impact. Third, organic materials have flexible molecular structures and can accommodate large Na-ions reversibly without much spatial hindrance, thus facilitating to achieve fast kinetics of Na insertion/extraction reaction. Fourth, structural diversity and easy control on functional groups make it straightforward to tailor organic materials' redox properties and electrochemical performances. Furthermore, the electroactivity of organic materials can be extended to other metal-ion battery systems because of the generality of their redox mechanisms. Therefore, in view of material sustainability and electrochemistry, it should be recognized that the application of OSIBs can combine the benefits of SIBs and organic materials, and eventually realize a truly 'green' EES technology.

Alongside the rapid development of inorganic SIBs during the past few years, a great amount of efforts has been devoted to organic electrode materials (Fig. 1b) so that OSIBs can be able to keep up with their inorganic counterpart on electrochemical performances, and be even better in some cases. On one hand, a wide range of organic molecules has been designed and proven to be redox active toward sodium. In principle, the redox reaction of organic molecules is based on the charge state change of the electroactive organic groups or moieties (Fig. 2). Carbonyl compounds are n-type organics and, depending on the redox potential, they can be used as either cathode or anode. Organic polymers (excluding polyimides and polyquinones) possess a bipolar nature but are preferentially used as p-type organics to obtain high discharge potential. Schiff bases and pteridine derivatives are newly emerged electrode materials and their electroactivity is based on the reduction of C=N bond. On the other hand, various electrode designs have been applied in OSIBs to solve the inherent problems of organic compounds, such as low electronic conductivity, pulverization, and solubility in organic electrolytes. Downsizing organic compounds to the nanometer scale can increase their electronic conductivity and accommodate large volume change associated with phase transition. Incorporating with carbon materials to form composite electrodes can potentially solve all three problems simultaneously. In particular, a variety of strategies have been proposed to reduce the solubility of organic compounds and crucial differences between OSIBs and OLIBs have gradually emerged alongside with the advance of OSIBs. Both aspects are worth further exploring.

It can be seen that the field of OSIBs is rapidly growing despite it is still in its early stage and a great progress has been made in the research community. Therefore, it is of great urgency and importance to summarize the progress and possibly draw general conclusions that could benefit the future advancement of this

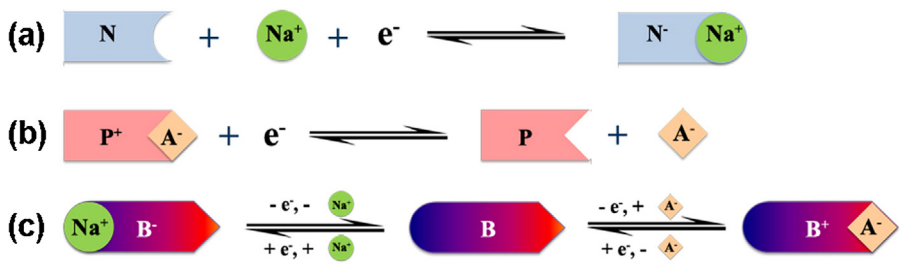

FIG. 2

The redox reaction of the n-type (a), p-type (b), and bipolar organics (c) in the Na system.

field. Indeed, several reviews can be found in the literature that contributes to OLIBs and SIBs with a primary focus on the electrode materials [1,8,20–25]. However, to the best of our knowledge, no review that covers both electrode materials and electrode structures in OSIBs has been published so far. Herein, we present in this review a comprehensive summary from the perspectives of molecular design and electrode design. In addition, solutions to the solubility issue and crucial differences between OSIBs and OLIBs are individually discussed. Furthermore, future challenges and opportunities in OSIBs are provided. We hope that this review can deliver a better understanding of the advantages of OSIBs and shed light on the applications of organic compounds in other possible energy technologies.

Molecular design

Carbonyl compounds

The carbonyl group is by far the mostly applied organic functional moiety in OSIBs owing to their high reactivity, fast kinetics, high capacity and a wide structural diversity. Almost all carbonyl compounds are n-type organics and one carbonyl undergoes a reversible one-electron reduction to form a monovalent anion that is balanced by a Na-ion and stabilized by structural substituents. According to the stabilizing mechanism, carbonyl compounds can be categorized into three types (Fig. 3). Type I compounds employ vicinal carbonyls to form stable enolates [26]. In Type II compounds, carbonyl groups are directly connected to an aromatic core which disperses the negative charge by delocalization [27,28]. This type of compounds includes aromatic carboxylates, imides and anhydrides. Type III compounds, most of which are quinones and ketones, share some characteristics with Type I and II compounds, but the main stabilizing force comes from the formation of extra aromatic system upon reduction [29,30]. The redox behavior of carbonyl compounds can be tuned by the inductive and resonance effect owing to their large structural variety. A major drawback is their solubility in organic electrolytes, thus how to reduce solubility has gained particular attention when applying them in OSIBs.

Carboxylates

The first example of carboxylates in OSIBs was disodium terephthalate (Na_2TP **1**, Fig. 4) simultaneously reported by two groups [31,32]. Na_2TP contains two carbonyl groups that allow inserting

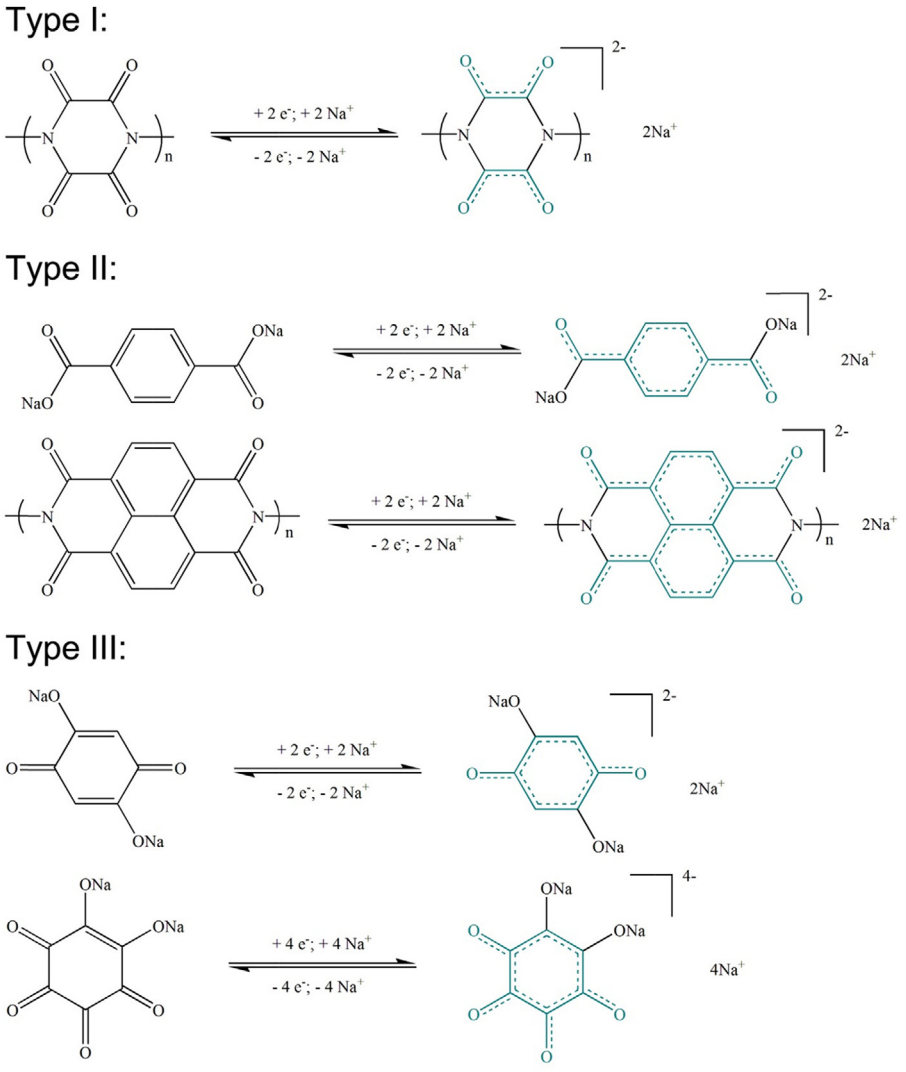

FIG. 3

Representative types of carbonyl compounds categorized according to the negative charge-stabilization mechanism.

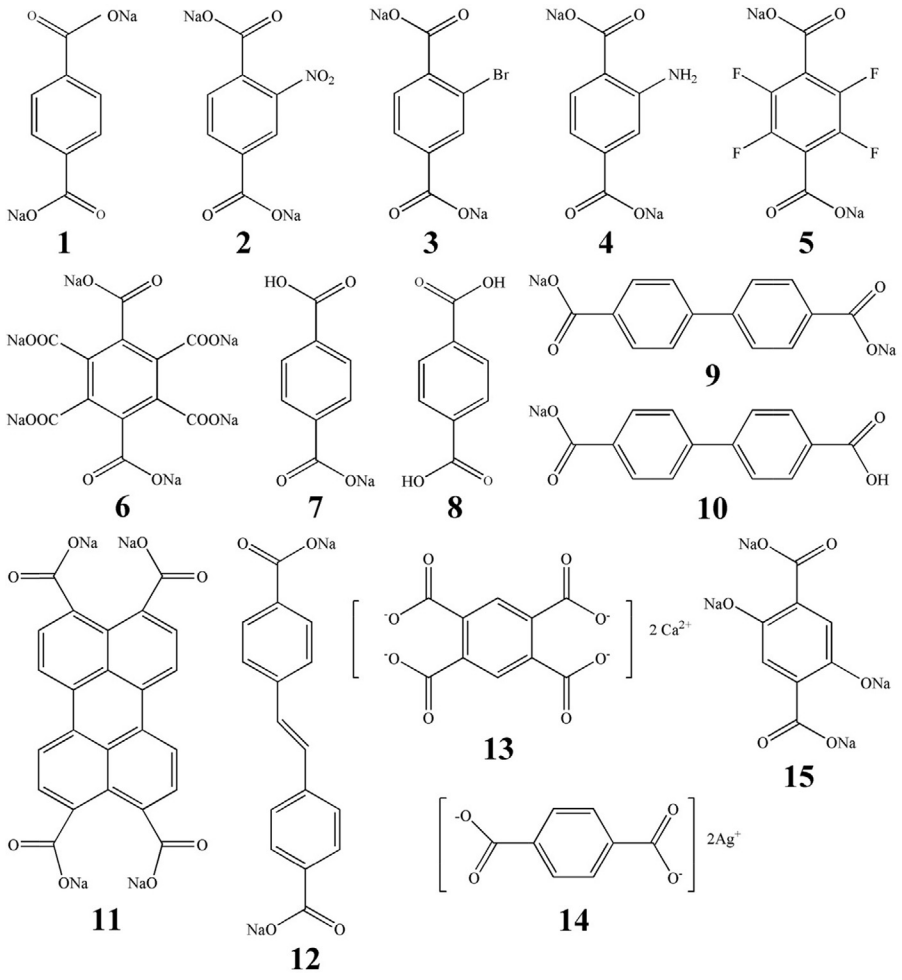

FIG. 4

Structures of carboxylates.

or extracting Na-ions, corresponding to a theoretical capacity of 255 mAh g^{-1}. It exhibited a discharge plateau locating at 0.3 V which is one of the lowest discharge voltages in OSIBs (Fig. 5a). Both groups reported a capacity close to the theoretical value at low rate during the initial cycles. Chen's group coated thin layer of Al_2O_3 (2 and 5 nm) on the electrode surface using atomic layer deposition (ALD) and obtained an improved capacity retention (82.7% after 60 cycles) (Fig. 5b) and rate capability (~150 mAh g^{-1} at 510 mA g^{-1}) [31]. Lee's group studied the inductive and resonance effect on the redox potential of Na_2TP using different substituents in the molecule [32]. The results showed that substituents with strong/weak electronegativity could withdraw/donate electron density from/to the conjugated carbon scaffolding and result in a higher/lower discharge voltage (NO_2-Na_2TP (**2**): 0.6 V, Br-Na_2TP (**3**): 0.5 V, and NH_2-Na_2TP (**4**): 0.2 V) (Fig. 5c and d). Abouimrane *et al.* reported similar effect on F-Na_2TP (**5**) and (COONa)-Na_2TP (**6**) with the discharge voltages of 0.6 and 0.5 V, respectively [33]. By contrast, no variation of discharge voltage was observed in the two protonated molecules, monosodium terephthalate (**7**) and terephthalate acid (**8**), which delivered capacities of 244 and 200 mAh g^{-1} at 10 mA g^{-1} after 50 cycles, respectively. However, the initial CE (ICE) decreased from 64% to 40% and 30% with from **1** to **7** and **8**. Same results were found in the sodium salts of 4,4′-biphenyldicarboxylate (Na_2BPDC **9**) and its partially deprotonated form (NaHBPDC **10**) [34]. Both materials exhibited a discharge capacity of ~200 mAh g^{-1} with a plateau at 0.5 V, but the ICE of **9** was significantly higher than **10** (81% vs. 47%).

According to Type II compounds, extending the conjugated system can increase the chemical stability and decrease the solubility of the compounds [35–40]. In sodium salt of 3,4,9,10-perylenetetracarboxylic acid (NaPTCDA **11**), the larger aromatic core enabled it stable cycle life over 300 cycles [35,36]. Wang *et al.* designed an extended π-conjugated system in sodium 4,4′-stilbene-dicarboxylate (SSDC **12**) [37]. The SSDC anode delivered a capacity of 204 mAh g^{-1} at 50 mA g^{-1} with a retention of 90% (Fig. 5e), and kept 70% of capacity at 1 A g^{-1} after 400 cycles. It also showed high rate capability, retaining the capacities of 110, 90 and 72 mAh g^{-1} at 2, 5 and 10 A g^{-1}, respectively (Fig. 5f). The extended π-conjugated system not only facilitates electron transport but also strengthens the intermolecular interactions by forming a layer-by-layer stacking which provides a Na-ion diffusion pathway. Another approach to reduce the dissolution of carboxylates is to form salts with inorganic cations that have high ionization energy with organic anions. Both organic calcium salt of 1,2,4,5-benzenetetracarboxylic acid (Ca_2BTEC

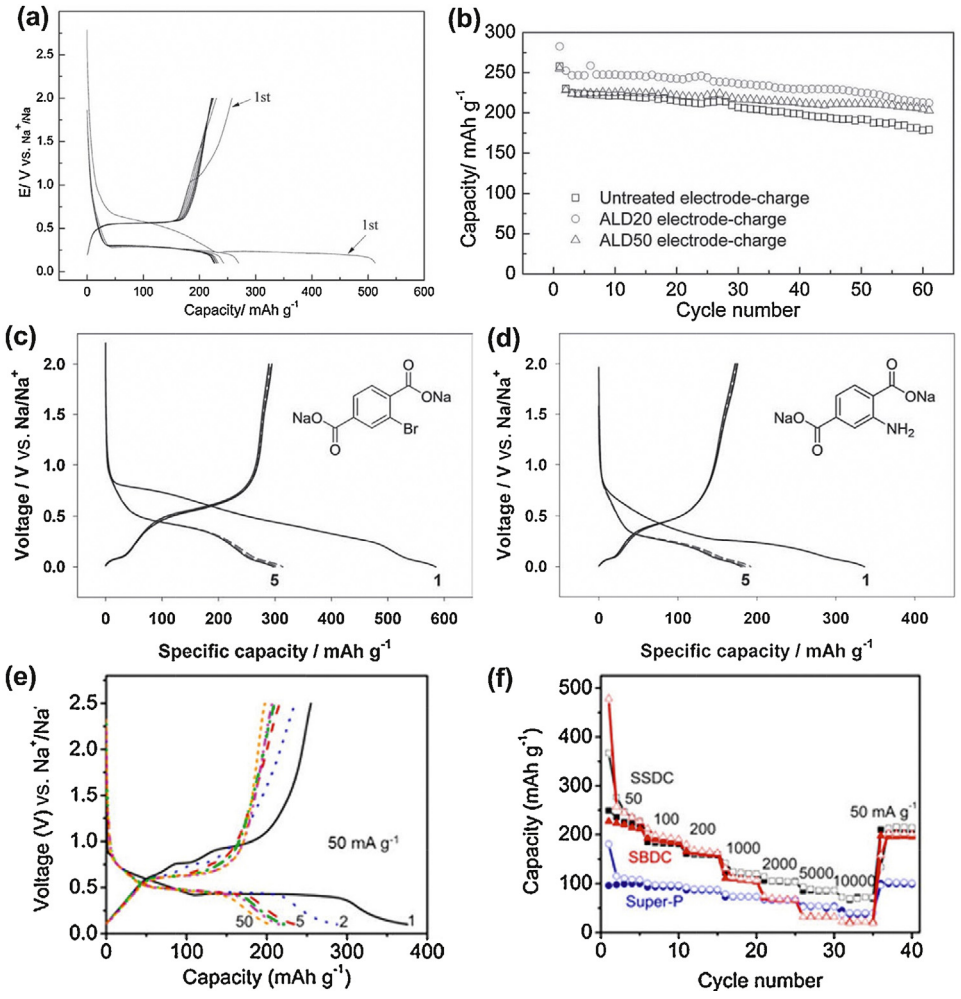

FIG. 5

(a) Charge–discharge curves of Na_2TP at 25.5 mA g^{-1}. (b) Cycling performance of the Na_2TP electrodes with and without ALD coating. Reproduced with permission [31]. Copyright 2012, Wiley-VCH. Charge–discharge curves of Br-Na_2TP (c) and NH_2-Na_2TP (d) at 30 mA g^{-1}. Reproduced with permission [32]. Copyright 2012, Wiley-VCH. Charge–discharge curves at 50 mA g^{-1} (e) and rate performance (f) of SSDC. Reproduced with permission [37]. Copyright 2015, American Chemical Society.

13) [41] and silver salt of terephthalate (Ag_2TP **14**) [42] exhibited stable cycle life over hundreds of cycles. In the case of Ag_2TP, the in situ generated Ag particles upon electrochemical reduction can enhance the conductivity of the electrode matrix.

Sodiation of small aromatic carboxylates typically proceeds at low potentials (<0.8 V vs. Na/Na^+) due to the electron donor group —ONa connected to the carbonyl, making carboxylates a promising class of anode materials in OSIBs and contributing to high energy density of full cells. A high working voltage of 3.6 V was realized by using Na_2TP as anode and $Na_{0.75}Mn_{0.7}Ni_{0.23}O_2$ as cathode and the full cell delivered 96% of its first discharge capacity after 50 cycles [33]. Substitution on aromatic cores strongly influents the redox behavior of carboxylates, providing a straightforward controllability of the electrochemical performances. In addition, dual functionality is possible if another functional group exists on the phenyl ring. For instance, tetrasodium salt of 2,5-dihydroxyterephthalic acid (Na_4DHTPA **15**) occupies carboxylate and Na-enolate quinone structure and can work as anode (discharge at 0.3 V) and cathode (discharge at 2.3 V) [43]. An all-organic full cell was built using Na_4DHTPA on both electrodes and displayed an average working voltage of 1.8 V and a capacity of ~150 mAh g^{-1} after 100 cycles. It is worth noting that the sodium plating potential is slightly below 0 V (vs. Na/Na^+), thus, the cut-off potential should be reasonably low to avoid sodium plating when applying sodiated carboxylates as OSIB anodes in a sodium half-cell.

Imides

The carbonyl groups in imides bound with nitrogen to form O═C—N and directly connect to an aromatic core. The redox mechanism of imides is based on an electrochemical enolization reaction of the carbonyl groups along with Na^+ associating with and disassociating from the oxygen atoms, during which the negative charge is stabilized by the aromatic core. Because of the high solubility, only two small diimide compounds have been reported in OSIBs so far [44,45]. The majority are dianhydride-derived polyimides (PIs), in which the electroactive monomer units were mostly 1,2,4,5-benzenetetracarboxylic dianhydride (PMDA **16**, Fig. 6) [46–48], 1,4,5,8-naphthalenetetra

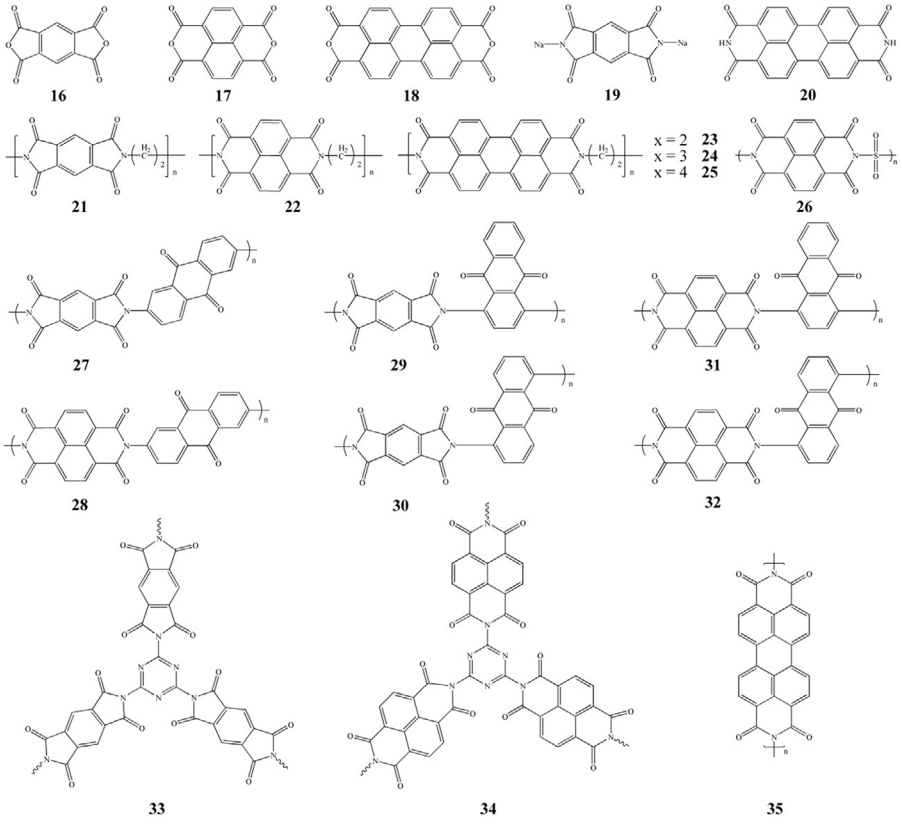

FIG. 6

Structures of anhydrides (**16–18**) and imides (**19–35**).

carboxylic dianhydride (NTCDA **17**) [46–50] and 3,4,9,10-peryle netetracarboxylic dianhydride (PTCDA **18**) [46,51].

Disodium salt of pyromellitic diimide (Na_2PMDI **19**) displayed multiple discharge plateaus appeared between 0.5 and 2 V, which is not appealing to full-cell applications [44]. It delivered a first discharge capacity of 191.3 mAh g^{-1} but showed poor capacity retention. Better retention was obtained from 3,4,9,10-perylene-bis(dicarboximide) (PTCDI **20**) which has a larger aromatic core with substantial electron mobility to facilitate the stabilization of the negative charge [45]. PTCDI delivered a capacity of 138.6 mAh g^{-1} and retained 77% after 300 cycles. Rate capability was demonstrated by maintaining 85% and 75% of the low-rate capacity at 300 and 600 mA g^{-1}.

PIs consisting of an electroactive center and an inactive linker were fabricated to avoid the unwanted dissolution appeared for small imides. Additional advantages such as high thermal stability and good mechanical properties could be achieved simultaneously. Wang *et al*. synthesized a series of PIs (**21-25**) and studied the dependence of electrochemical performance on the dianhydride [46]. By altering the electroactive core, the average discharge voltage increased from 1.73 (**21**) to 1.89 (**22**) and 1.94 V (**23**) and cycling stability was enhanced owing to the reduced solubility (Fig. 7a). Decreasing the alkyl chains (**23-25**) led to decreased molecular weight, thereby increasing the capacity. **23** delivered the capacities of 137.6 mAh g^{-1} at 25 mA g^{-1} after 400 cycles and 110.8 mAh g^{-1} at 200 mA g^{-1} after 5000 cycles as well as an impressive rate capability (50 mAh g^{-1} at 10 A g^{-1} and 38.9 mAh g^{-1} at 20 A g^{-1}) (Fig. 7b and c). Using electron-withdrawing sulfonyl as linker (**26**), the voltage was increased to 2.3 V comparing with **22** because of the inductive effect [50]. Redox-inactive alkyl and sulfonyl groups can be replaced by redox-active fragments to avoid capacity loss. Anthraquinone (AQ) was used to link PMDA or NTCDA to form conjugated poly (anthraquinonyl imide) (PAQI, **27-32**). The polymers showed a capacity of ~200 mAh g^{-1} at 50 mA g^{-1}, corresponding to more than three-electron transfer per molecular unit [47,48]. Their cyclability was dependent on the isomerism of the AQ fragments due to the steric hindrance for Na-insertion and solubility of the polymers, with **31** exhibiting the highest retention of 95% over 150 cycles. In addition, PIs with a three-dimensional (3D) cross-linked network (**33** and **34**) possess enhanced electron and ion transport derived from the 3D conjugated system, thereby exhibiting high rate capability [52].

In principle, each diimide or polyimide should be able to transfer four electrons per formula or unit upon full sodiation. Four negative charges introduced into the aromatic system is most likely to create a high-energy configuration that, in turn, could trigger side-reactions, causing a severe structural damage or even decomposition. Thus, imides can only realize a two-electron redox reaction at an acceptably potential range (>1.5 V) according to the reported capacities so far. Although the moderate voltage (1.5–2.3 V) makes imides not an ideal candidate on either end, it makes imides versatile to pair with various materials. Full cells using PTCDA-derived PI (**35**) as cathode [51] or NTCDA-derived PI (**22**) [49] as anode both delivered a working voltage of 1.2–1.4 V. Furthermore, tuning the

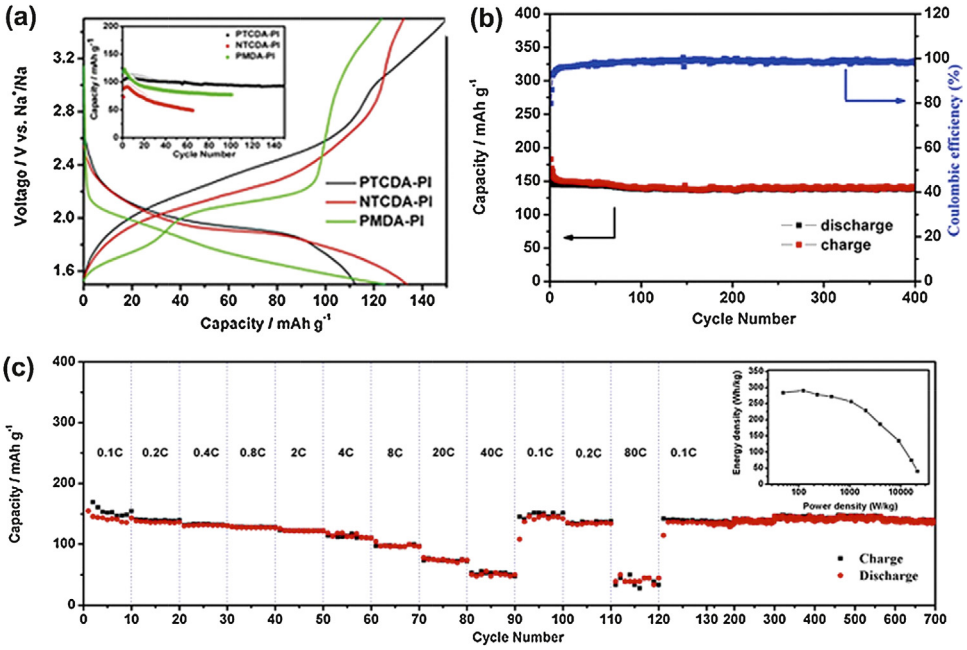

FIG. 7

(a) Charge–discharge curves of different dianhydride-derived PIs at 25 mA g^{-1} (inset: cycling performance). Cycling performance at 25 mA g^{-1} (b) and rate performance (c, inset: Ragone plots) of the PTCDA-derived PI. Reproduced with permission [46]. Copyright 2014, Wiley-VCH.

redox-reactive centers and linking fragments in PIs could maximize the controllability of their electrochemical performances, the ease of which holds great advantage against inorganic SIB electrode materials.

Anhydrides

Study of anhydrides in OSIBs has been performed alongside with diimides and the studied materials had high resemblance on molecular structures between the two classes. Two groups have investigated the battery performance and electrochemical mechanism of PTCDA (**18**, Fig. 6) and reported that PTCDA underwent a three-step sodiation process when discharging to 0.01 V, corresponding to 15 Na-ions insertion [53,54]. But the complete uptake of 15 Na-ions could destroy the crystal structure of PTCDA and lead to a poor reversibility. In a range of 1–3 V, PTCDA delivered a capacity of 145 mAh g^{-1} at 10 mA g^{-1}, a rate capability of 91 mAh g^{-1} at 1 A g^{-1}, and good cycling stability over 200 cycles [53]. Unlike PTCDA, its tetrasodium salt NaPTCDA (**11**) exhibited a capability of only two-Na uptake even at deep-discharge condition [36,54], implying that the backbones of NaPTCDA are not able to support more Na-ions due to the steric hindrance. Other anhydrides such as PMDA (**16**)

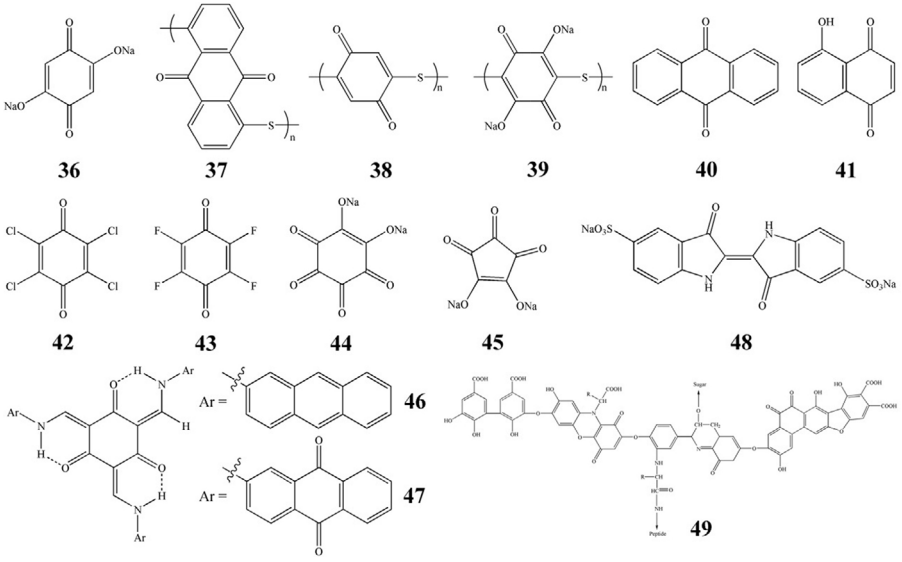

FIG. 8

Structures of quinones (**36–43**) and ketones (**44–49**).

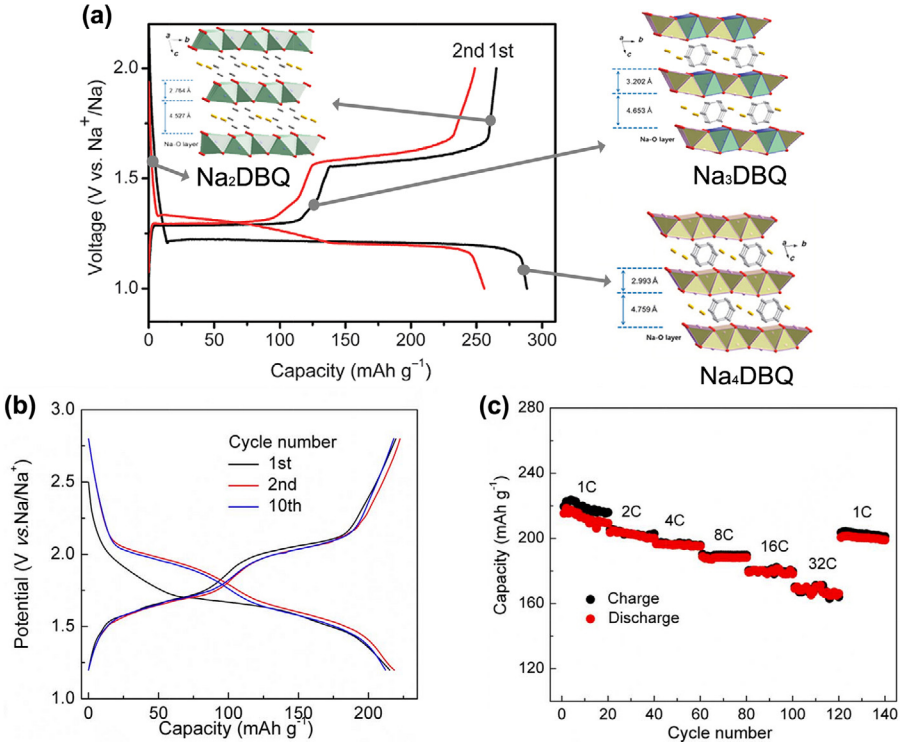

FIG. 9

(a) Charge–discharge curve of Na_2DBQ at 29 mA g^{-1} and its phase change during the first cycle. Reproduced with permission [57]. Copyright 2015, AAAS. Charge–discharge curves at 180 mA g^{-1} (b) and rate capability of PAQS (c). Reproduced with permission [59]. Copyright 2013, Nature Publishing Group.

and NTCDA (**17**) displayed similar electrochemical behavior as PTCDA [54].

Quinones

Quinones belong to Type III compound and the stabilization of the negative charge upon reduction of the carbonyl group lies on the formation of an additional aromatic system. This class of materials suffers serious solubility in organic electrolytes, so reducing solubility has been in the center of focus. Disodium salt of 2,5-dihydroxy-1,4-benzoquinone (Na_2DBQ **36**, Fig. 8) has two carbonyl groups that realizes two Na-ions uptake [55–58]. Its structure consists of inorganic Na—O polyhedral layer and organic π-stacked benzene layer. The former provides conduction pathways and storage sites for Na-ions and the latter is responsible for the conduction and storage of electrons. Zhu *et al.* reported a high capacity (265 mAh g^{-1} at 29.1 mA g^{-1}), a long cycle life (181 mAh g^{-1} after 300 cycles), and a good rate capability (~160 mAh g^{-1} at 1.45 A g^{-1}) [56]. Luo *et al.* deposited a thin Al_2O_3 layer (2 nm) on the Na_2DBQ electrode using ALD and obtained an improved cyclability of 212 mAh g^{-1} at 50 mA g^{-1} after 300 cycles with CE almost reaching 100% [55]. Wu *et al.* introduced carbon nanotubes (CNTs) to immobile Na_2DBQ and decrease its dissolution, and the composites delivered the capacities of 161 and 142 mAh g^{-1} at 1.45 and 2.03 A g^{-1}, respectively [58]. All above works have seen an 'activation' process that Na_2-DBQ underwent during the initial cycle. Hu and his coworkers revealed that this process was related to an intermediate phase Na_3DBQ in the first desodiation (Fig. 9a) and proposed a storage mechanism based on it [57].

Another approach to overcome the dissolution problem of small molecule quinones is to incorporate the quinone structures into a polymeric moiety. Deng *et al.* synthesized poly(anthraquinonyl sulfide) (PAQS **37**) that contains abundant redox-active AQ units linked by thioether bonds [59]. The polymer delivered a capacity of 220 mAh g^{-1} with two sequential plateaus at 1.5 and 2.0 V, corresponding to 98% theoretical capacity (Fig. 9b). It maintained the capacities of 175 and 160 mAh g^{-1} at 3.2 and 6 A g^{-1}, respectively, representing one of the best rate capabilities of quinones (Fig. 9c). Moreover, a stable cyclability with 85% capacity retention over 500 cycles at 1.6 A g^{-1} was also obtained. In a similar spirit, insoluble poly(benzoquinonyl sulfide) (PBQS **38**) reported by Zhou's group exhibited an initial capacity of 247 mAh g^{-1} at 50 mA g^{-1} with 74% retention after 100 cycles [60]. By introducing the electron-donating —ONa group into benzene ring, the obtained sodium salt of poly(2,5-dihydroxy-*p*-benzoquinonyl sulfide) (Na_2PDS **39**) exhibited a lower discharge voltage of 1 V [61]. In addition, approaches involving carbonaceous materials have been prove effective to reduce the dissolution of quinone-based materials, such as encapsulating AQ (**40**) in mesoporous carbon [62] and immobilizing Juglone (**41**) on reduced graphene oxide (rGO) nanosheets [63], which will be discussed in the section of 'Electrode design'.

Small quinone-based molecules have drawn increasingly attention in OSIBs due to their relatively high redox reactivity, tunable redox behavior, and high theoretical capacities derived from low molar mass. To solve the dissolution problem, incorporating quinonide structures into an insoluble polymeric framework seems very promising. However, the relatively low

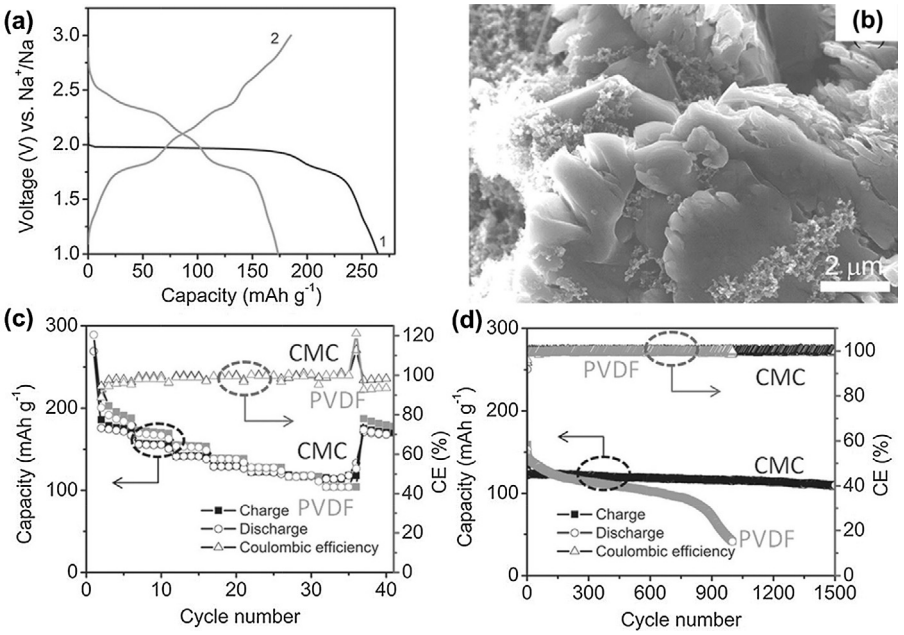

FIG. 10

(a) Charge–discharge curve of the first cycle of DSR at 50 mA g^{-1}. (b) SEM image of DSR after discharging to 1.5 V. Rate performance (c) and cycling performance at 1 A g^{-1} (d) of the DSR electrodes using CMC or PVDF as binder. Reproduced with permission [67]. Copyright 2016, Wiley-VCH.

discharge voltage as cathodes (<2.2 V) is not favorable to achieve high energy density of full cells. Kim *et al.* proposed quinone-derivative cathodes using the halogen substituents with strong electron-withdrawing property [64]. The inductive effect boosted the discharge voltage, reaching 2.72 V in $C_6Cl_4O_2$ (**42**) and further to 2.9 V in $C_6F_4O_2$ (**43**). It is reasonable to expect that using electron withdrawal from active redox centers in the polymers might be able to simultaneously provide high cycling stability and operating voltage.

Ketones

Ketones can be electrochemically reduced to the corresponding alcohols and reoxidized to their original state, realizing a one-electron redox reaction. Disodium salt of rhodizonate (DSR **44**, Fig. 8) has four carbonyl groups per formula with a high theoretical capacity of ~500 mAh g^{-1}. Okada's group first used DSR in OSIBs and obtained a capacity of ~150 mAh g^{-1} at 18 mA g^{-1} after 40 cycles [65]. A plateau at 2.0 V appeared in the first sodiation but changed to stepwise curves in the following cycles, indicating an activation process. Yu and his coworkers attributed this activation process to the stress/strain induced in the first sodiation at overpotential due to a large volume expansion [66]. Their DFT simulation results showed that the uptake of Na^+ may take place at four different carbonyl groups according to the similar bonding energies, thus DSR may undergo a sequential one-electron reduction process at different potentials or two-electron process, corresponding to the stepwise voltage plateaus. Wang *et al.* observed that, after the activation process, cracks cause by volume change appeared on the surface of DSR and a flaky morphology formed (Fig. 10a and b) [67]. The flaky morphology was the external refection of the internal layer-by-layer molecular arrangement, which resembles the common feature of the layered inorganic cathode materials with an open structure that could facilitate Na-ion diffusion in between adjacent layers. DSR delivered capacities of 173.5 and 115 mAh g^{-1} at 50 mA g^{-1} and 5 A g^{-1}, respectively (Fig. 10c), and exhibited a long-term cycling stability by retaining a capacity of 110 mAh g^{-1} after 1500 cycles at 1 A g^{-1} (Fig. 10d). Croconic acid disodium salt (CADS, **45**) has a similar structure with DSR and, as a result, experienced large volume change in the initial cycle. Luo *et al.* encapsulated it with GO to alleviate the volume change and obtained better cyclability than the bare counterpart [68]. Besides the volume change and pulverization, the α-C radical intermediates generated during the sodiation/desodiation process is another possible issue of ketones with high density of carbonyl groups in OSIBs because the radical intermediates could induce undesired side reactions, eventually leading to irreversibility of the redox process and disappointing cyclability. Lu's group designed the tri-carbonyl-based tris N-salicylideneanthramine (TSAA **46**) and tris N-salicylideneanthraquinoylamine (TSAQ **47**) which showed excellent reversible transformation between C═O and C—O—Na because the reactivity of the α-C radical intermediates were largely suppressed by an electronic resonance effect and steric hindrance from the substitution groups [69]. TSAQ delivered capacities of 370 and 220 mAh g^{-1} at 50 mA g^{-1} and 1 A g^{-1}, respectively, and showed no obvious capacity degradation after more than 2500 cycles at 1 A g^{-1}.

Yao *et al.* reported that indigo carmine (IC **48**), a water-soluble organic molecule widely used as a food dye, can act as an OSIB cathode owing to its very low solubility in ordinary organic solvents derived from the peripheral polar sulfonate groups (—SO_3Na) [70]. IC exhibited a capacity of 106 mAh g^{-1} at 10 mA g^{-1} with an average voltage of 1.8 V, being close to its theoretical capacity, and dropped only 20 mAh g^{-1} after 40 cycles with an almost 100% CE. A natural polymer humic acid (HA **49**) was tested as an OSIB anode and showed reversible Na

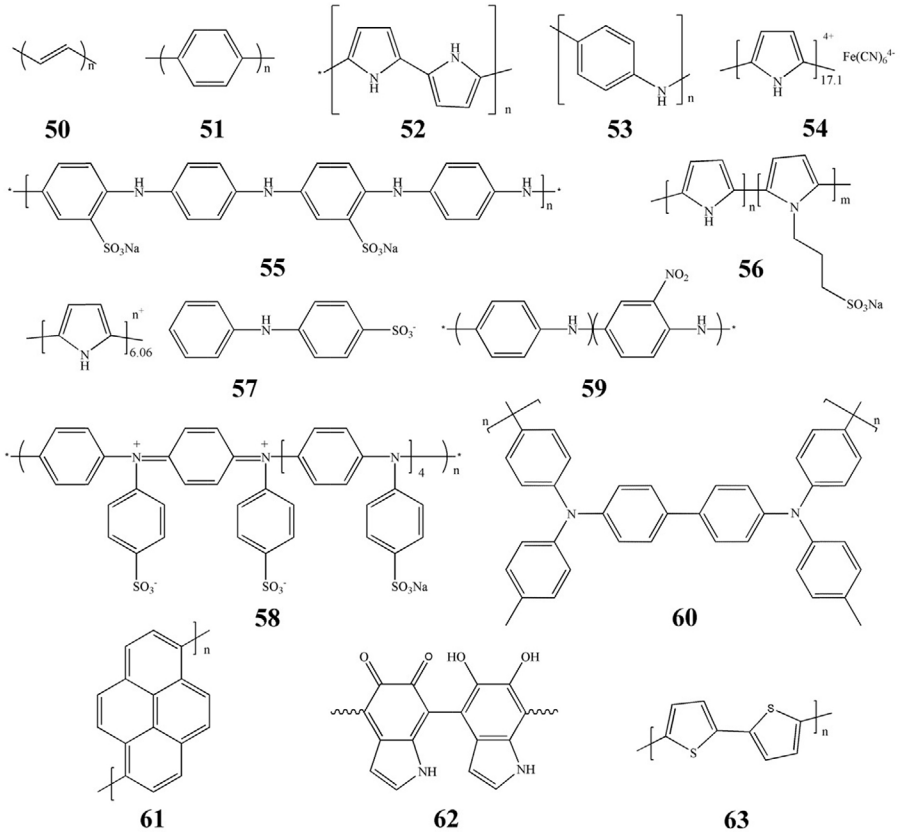

FIG. 11

Structures of conductive polymers.

insertion/extraction centered at 0.48/0.71 V. A comparably large first discharge capacity of 244 mAh g^{-1} at a low rate but low capacity retention was observed at high rates [71].

Organic polymers

Conductive polymers

Conductive polymers (CPs) are the first type of organic materials used in OSIBs. In 1985, Shacklette *et al.* examined polyacetylene (PAc **50**, Fig. 11) and poly(*p*-phenylene) (PPP **51**) and demonstrated their Na-ion storage ability (~1.5 V) at their reduced states [72]. Polypyrrole (PPy **52**)- [73–78] and polyaniline (PAn **53**)-based CPs [59,79–83] are two typical examples that have been widely studied so far. They were usually as-synthesized in the p-doped state underwent a p-doping/de-doping mechanism with large electrolyte anions, which suffers a low doping degree and poor capacity utilization of the polymer chains. In addition, all the p-doped polymers are virtually not Na-storage hosts and cannot form a classic 'rocking chair' SIBs. An effective way is to incorporate redox-active species into the polymer chains where they can contribute their redox capacity. Inorganic redox-active ferricyanide anions were doped into the PPy matrix and the obtained PPy/FC (**54**) exhibited enhanced capacities of 135 mAh g^{-1} at 50 mA g^{-1} with 85% retention over 100 cycles (Fig. 12a) [73]. Poly(aniline-*co*-aminobenzenesulfonic sodium) (PANS **55**) synthesized by grafting the —SO_3Na group onto the PAn chains showed similar capacity with 96.7% retention over 200 cycles [79]. Doping with organic redox species, poly (pyrrole-*co*-(sodium-3-(pyrrol-lyl) propanesulphonate)) (PPy-PS **56**) [74], diphenylamine-4-sulfonate-doped PPy (PPy/DS **57**) [75], and poly(diphenylaminesulfonic acid sodium) (PDS **58**) [80] were obtained. PPy/DS showed a capacity of 115 mAh g^{-1} at 50 mA g^{-1} with 82% retention over 50 cycles and PDS displayed a high voltage of 3.4 V owing to the high redox potential of the diphenylamine moiety (Fig. 12b).

Benefiting from the high redox potential of the CPs, all-organic SIBs can be built using n-type organics as anodes. An all-solid-state full cell consisting of aniline/*o*-nitroaniline (PANA **59**) and PAQS displayed a voltage of ~1.6 V and a capacity of ~200 mAh g^{-1} with 80% retention after 50 cycles (Fig. 12c) [81,82]. It also demonstrated a rate capability with a 60% capacity retention at a rate of 800 mA g^{-1} (Fig. 12d). Polytriphenylamine (PTPAn **60**) exhibited a high voltage (~3.6 V), a 90% theoretical capacity (~100 mAh g^{-1}), a great rate capability (88 mAh g^{-1} at 2 A g^{-1}), and a stable cycle life (97% retention after 200 cycles at 500 mA g^{-1}) [59]. Paring PTPAn with PAQS, the full cell displayed an average voltage of 1.8 V and capacities of 130 and 118 mAh g^{-1} at 3.2 and 6.4 A g^{-1}, respectively. A similar high discharge voltage of 3.5 V was found in the non-crystalline oligopyrene (OPr **61**) [84].

Polydopamine (PDA **62**) was newly investigated in OSIBs because of its interesting molecular structure where the carbonyl groups exhibit n-type behavior while the secondary amine (R-NH-R) adopts p-doping/de-doping characteristic, making PDA versatile to be either anode or cathode depending on the applied potential window. PDA showed so far the best electrochemical performances among all the CPs, delivering a capacity of

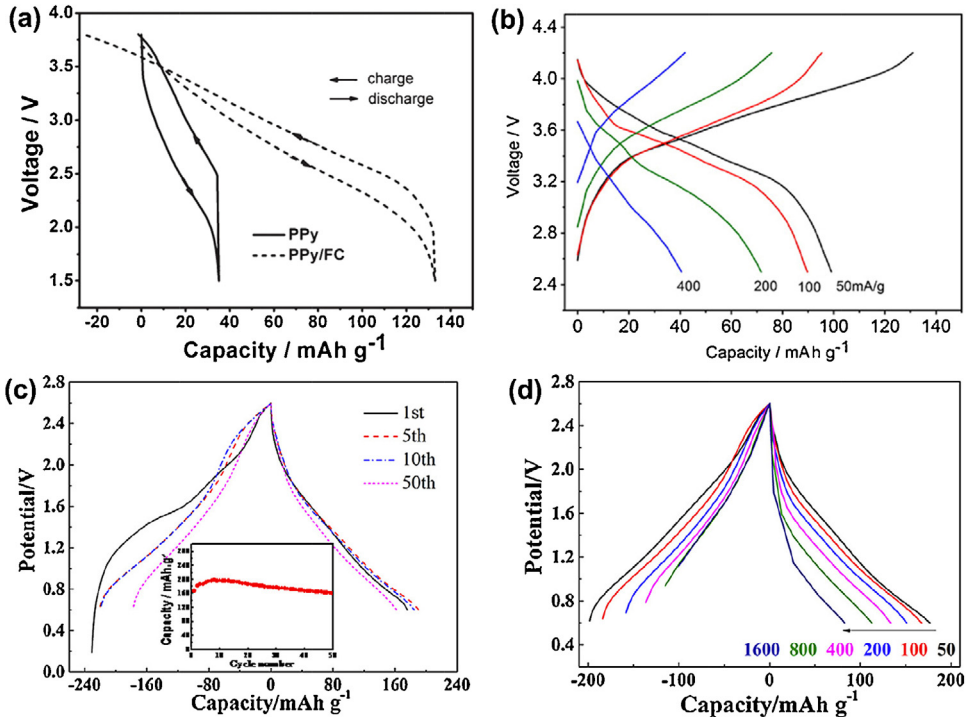

FIG. 12

(a) Charge–discharge curve of PPy and PPy-FC at 50 mA g^{-1}. Reproduced with permission [73]. Copyright 2012, Royal Society of Chemistry. (b) Charge–discharge curves of PDS at different rates. Reproduced with permission [80]. Copyright 2014, Elsevier. (c, d) Charge–discharge curves of the all-solid-state P(An-NA)/PAQS full cell at different current densities. Inset in (c) is the cycling performance at 50 mA g^{-1}. Reproduced with permission [82]. Copyright 2015, Elsevier.

~500 mAh g^{-1} after 1024 cycles at 50 mA g^{-1} as anode [85] and sustaining a high rate of 10 A g^{-1} as cathode [86]. Polybithiophene (PBT **63**) was another reported CP that showed n-type redox reversibility and underwent doping/de-doping reaction with Na^+ [87].

As seen, the greatest strength of CPs is their high electronic conductivity and high redox potential while the major drawback is the undefined discharge plateaus and comparably low specific capacities due to the low density of active sites in the polymeric backbones, causing the energy density to be on the lower end. Another critical point is that the cyclability of CPs are sensitive to the upper cut-off voltage as over-oxidization at high voltage could cause unstable structures or even decomposition due to the serious charge repulsion interaction between structural units. As the p-doping process shows a typical capacitive response, the electrochemical performance can be promoted by enhancing surface area through nanostructuring [76–78], which will be discussed in the section of 'Electrode design'. In addition, the

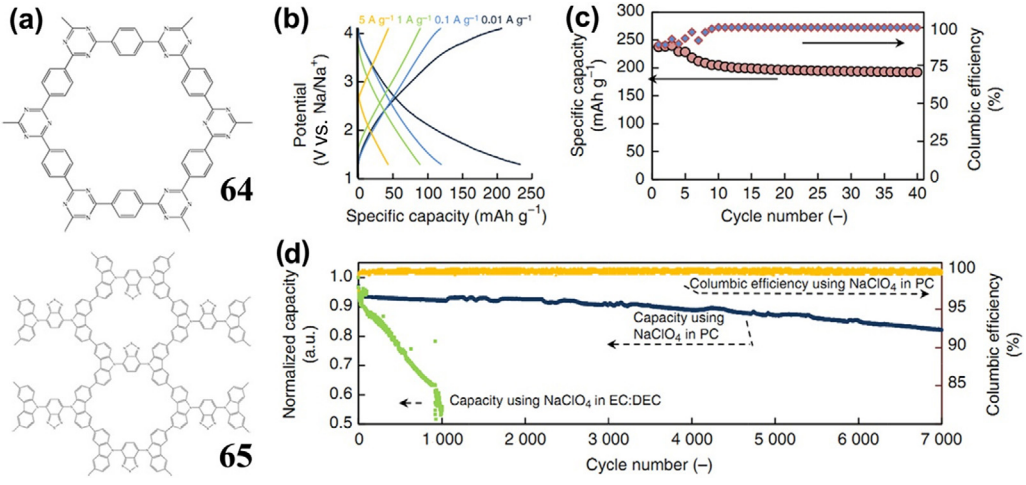

FIG. 13

(a) Structures of conjugated microporous polymers. Charge–discharge curves at different rates (b) and cycling performance at 10 mA g^{-1} (c) and 1 A g^{-1} (d) of BPOE. Reproduced with permission [88]. Copyright 2013, Nature Publishing Group.

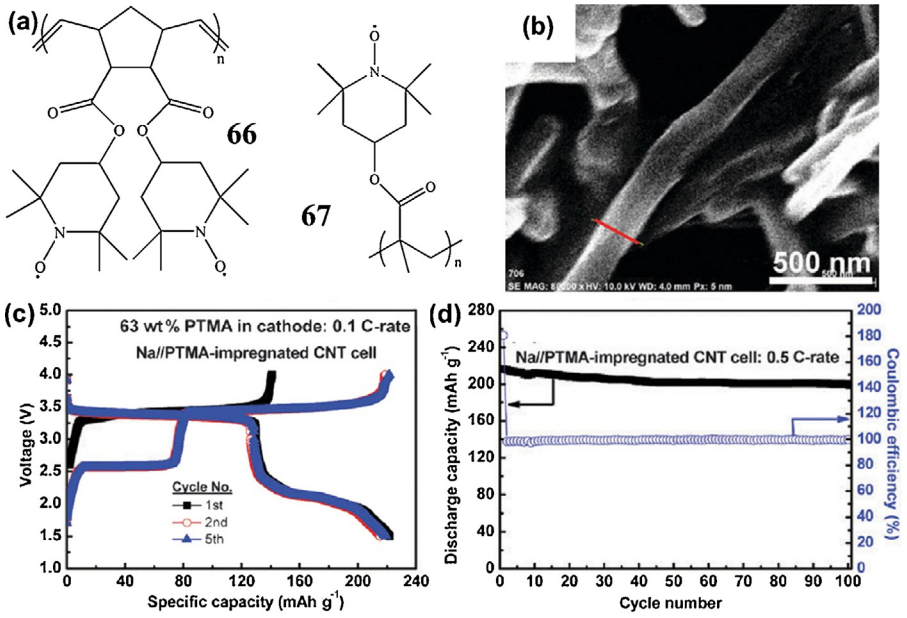

FIG. 14

(a) Structures of nitroxyl radical polymers. SEM image (b), charge–discharge curves (c), and cycling performance (d) at 0.1 C of the PTMA-impregnated CNTs electrode. Reproduced with permission [95]. Copyright 2015, Royal Society of Chemistry.

self-discharge issue is often associated with the CP electrodes and could be caused by the capacitive controlled response, over-oxidation, or dissolution in electrolytes. Thus proper material or electrode designs should be taken into considerations to avoid the self-discharge issue when applying CPs in SIBs.

Conjugated microporous polymers

Conjugated microporous polymers are of great interest because they combine high surface area with intrinsic advantages relevant to the π-conjugated skeletons. A bipolar porous organic electrode (BPOE **64**, Fig. 13a) was fabricated by Sakaushi *et al*. for Na storage [88,89]. It is a short-range-ordered 2D polymeric framework consisting of benzene rings and triazine rings in a porous-honeycomb structure, displaying a sheet-like morphology with micropores of ca. 1.4 nm. BPOE had a p-dopable region (with ClO_4^-) above 2.8 V and an n-dopable region (with Na^+) below 2.8 V, and the two doping processes can be continuously and linearly connected. Therefore, a capacity over 200 mAhg^{-1} was obtained in a range of 1.3–4.1 V and 80% retention was observed after 7000 cycles at 1 A g^{-1} (Fig. 13b–d). The porous framework of BPOE can facilitate electrolyte filtration and ion transport, resulting in a high rate capability (~50 mAh g^{-1} at 5 A g^{-1}). A very high surface area of 1166 m^2 g^{-1} and micropores of 0.52 and 0.86 nm was obtained from 4,7-dicarbazyl-[2,1,3]-benzothiadiazole (PDCzBT **65**) and it delivered capacities of 145 mAh g^{-1} after 100 cycles at 20 mA g^{-1} and 99 mAh g^{-1} after 200 cycles at 100 mA g^{-1} [90].

Nitroxyl radical polymers

Organic radical polymers (ORPs) have pendant side groups consisting of stable organic radicals and present the highest redox potentials among OSIB materials. ORPs have been advanced in OLIBs [91–93], but only two examples were reported in OSIBs, both of which adopted nitroxyl radical 2,2,6,6-tetramethyl-1-pi peridinyloxy (TEMPO) in their repeating unit [94,95]. TEMPO shows a bipolar nature and can be either oxidized to an oxoammonium cation or reduced to an aminoxy anion through a one-electron redox reaction. Poly[norbornene-2,3-endo,exo-(COO-4-TEMPO)$_2$] (**66**, Fig. 14a) displayed a high discharge plateau of 3.44 V provided by the oxidization of TEMPO but showed

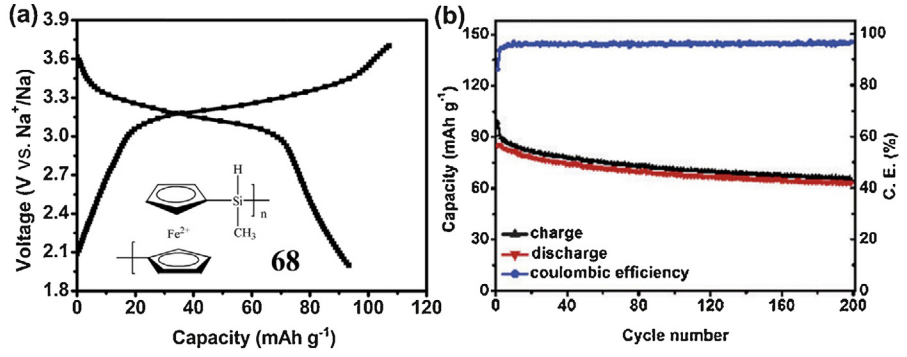

FIG. 15

(a) Charge–discharge curves of PFS (inset: structure of PFS). (b) Cycling performance at 5 C of the PMDA/PFS full cell. Reproduced with permission [96]. Copyright 2014, Royal Society of Chemistry.

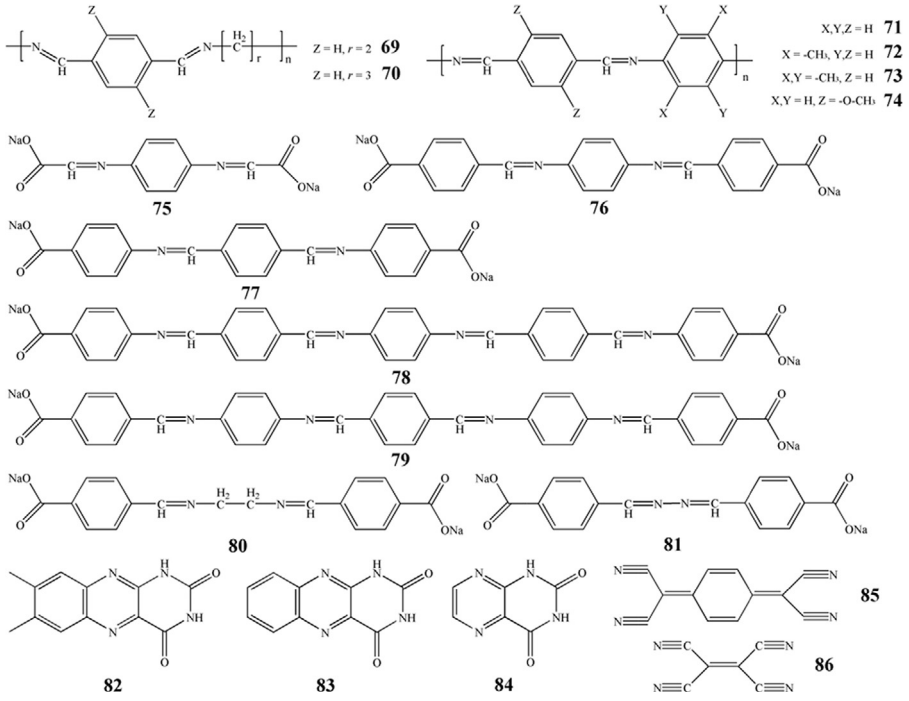

FIG. 16

Structures of Schiff bases (**69–81**) and pteridine derivatives (**82–86**).

high irreversibility in the initial cycles [94]. ORPs are mostly subjected to a high self-discharge because of the easy dissolution in organic electrolytes, and their high insulating characteristic deteriorates energy density. Kim *et al.* encapsulated poly(2,2,6,6-tetra methylpiperidinyloxy-4-vinylmethacrylate) (PTMA **67**) into CNTs to reduce the dissolution of PTMA and introduce an electronic conduction network (Fig. 14b) [95]. The encapsulated PTMA delivered a high capacity of 222 mAh g^{-1} at 0.1 C rate with 93% retention after 100 cycles and 190 mAh g^{-1} at 5 C rate (Fig. 14c and d). Two plateaus at 3.36 and 2.1 V were observed corresponding to the p- and n-doping process of TEMPO, respectively.

Organometallic polymers

Organometallic polymers contain electroactive organometallic redox moieties that are responsible for the electrochemical activity. Poly(ferrocenyl-methylsilane) (PFS **68**, Fig. 15a) was reported as an OSIB cathode material based on the fast electrochemical response of ferrocene [96]. The ferrocene moiety was bridged to the polymer backbones by silicon and displayed a p-doping/de-doping behavior with ClO_4^- in the electrolyte accompanying the redox reaction between Fe^{2+} and Fe^{3+}. PFS exhibited an average discharge voltage of 3.2 V with a negligible voltage gap between charge and discharge (Fig. 15a). An all-organic full cell was demonstrated by paring PFS with a polymer anode and it delivered an average discharge plateau of 1.2 V and a first discharge capacity of 85 mAh g^{-1} with 74% retention after 200 cycles (Fig. 15b).

Schiff bases

Organic compounds with promising anode performance are so far limited to carboxylates. A new candidate for anode based on the Schiff base functionality ($R^1HC{=}NR^2$) was recently demonstrated [97]. The reported polymeric Schiff bases (**69-74**, Fig. 16) have in common an active Hückel group, —N=CH—ϕ—HC=N— (ϕ: phenyl group) with 10 π-electrons, that is capable of inserting more than one Na^+ per —C=N— bond. The electrochemical activity can be tuned by using aromatic and nonaromatic diamine blocks between the terephthalaldehyde monomer units and adding donor substituents on the anil and benzyl rings. Conjugated Schiff bases (**71-74**) showed more stable activity and higher capacity retention below 1 V than non-conjugated ones (**69**, **70**). Best performance was obtained from **71**, delivering a capacity of 350 mAh g^{-1} with a Na insertion voltage of 0.65 V. The same group also reported the Na storage of oligomeric Schiff bases with carboxylate end groups (**75-81**) and demonstrated the voltage control by pure carboxylates (**76**), pure Schiff bases (**77**, **78**), or combined (**79**) electrochemical mechanism [98]. The DFT calculations determined that the active Hückel co-planar units ($—^-OOC—ϕ—C{=}N—$ and —N=C—ϕ—C=N—) were responsible for Na^+ insertion, whereas the isoelectronic groups ($—^-OOC—ϕ—N{=}C$ and —C=N—ϕ—N=C—) were not active but had a stabilizing effect by either favoring the π–π interactions or avoiding N—N repulsions and loss of planarity. Lack of the stabilizing effect resulted in a lowered discharge voltage (**80**, **81**). The oligomeric Schiff bases presented a low discharge voltage (<1.2 V), high capacities (up to 340 mAh g^{-1}), and high CE (>98% after a few cycles).

Pteridine derivatives

The use of biologically occurring redox centers holds a great potential in designing OSIB materials. Inspired by the heterocyclic molecules that contain a pteridine (1,3,5,8-tetraazanaphthalene) nucleus, Hong *et al.* first presented the

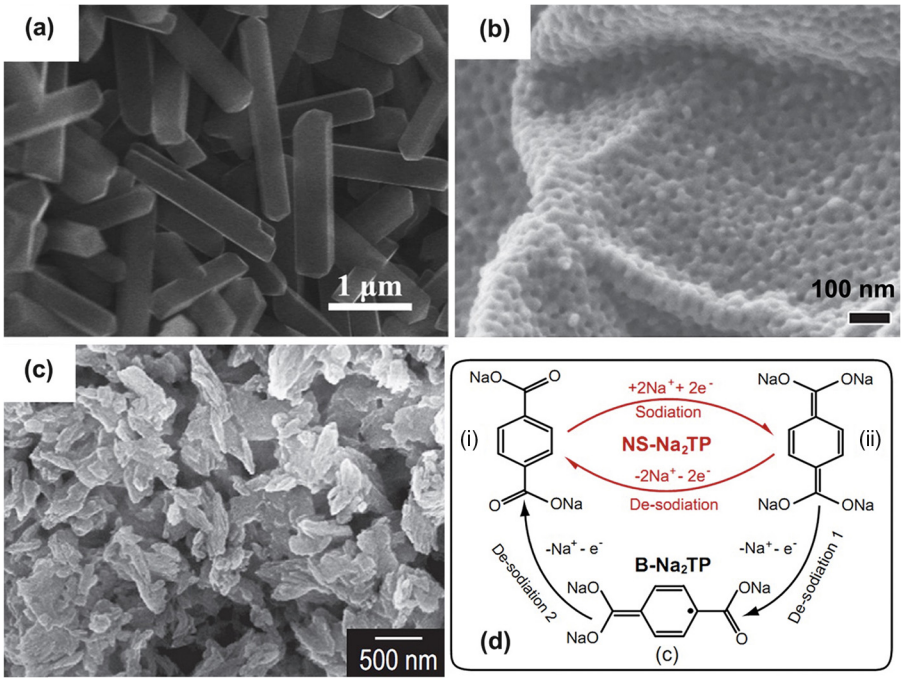

FIG. 17

(a) SEM image of the DSR nanorods. Reproduced with permission [66]. Copyright 2016, American Chemical Society. (b) SEM image of 2D mesoporous PPy nanosheets. Reproduced with permission [77]. Copyright 2016, Wiley-VCH. (c) SEM image of the Na_2TP nanosheets. (d) Illustration of the possible charge/discharge mechanisms of the Na_2TP nanosheets and bulk. Reproduced with permission [107]. Copyright 2015, Elsevier.

pteridine derivatives in the alloxazinic structure as cathodes [99]. The redox activity lies on the conjugated diazabutadiene region that facilitates the electron transfer reaction upon reduction of nitrogen. Lumichrome (**82**, Fig. 16), alloxazine (**83**) and lumazine (**84**) were capable of reversibly inserting/extracting two Na-ions and delivering capacities of 138, 168 and 70 mAh g^{-1} at 20 mA g^{-1}, respectively, which could be increased to 220–250 mAh g^{-1} if incorporating CNTs. However, limited cyclability was observed due to the large strain deriving from large sized Na-ions. Besides C=N bonds, C≡N bonds were both experimentally investigated for Na storage in tetracyanoquinodimethane (TCNQ **85**) [100] and computationally studied by using tetracyanoethylene (TCNE **86**) as an example [101,102].

Electrode design

Organic compounds as SIB electrodes face three major challenges: (1) the intrinsically low conductivity reduces reaction kinetics, resulting in large overpotential and unsatisfactory rate capability; (2) material pulverization induced by large volume change during phase transition causes rapid capacity decay; (3) easy dissolution in organic electrolytes leads to loss of active materials upon cycling, contributing to capacity loss. Alongside with discovering new organic molecules, rationally designing electrodes has drawn particular attention to meet the challenges. In this section, we will summarize the effective electrode designs in two categories: nanoeffects and composites with carbon materials.

Nanoeffects

Applying nanostructures in OLIBs has offered the opportunity to develop electrodes with large capacity, high energy and power density, and long cycle life [103–106]. Investigations on nanoeffects in OSIBs are limited, but promising results have been achieved over different types of compounds such as carboxylates, ketones and CPs. Besides the general merits such as facile electron transfer, easy Na-ion diffusion, and numerous active sites [32,38,55,76,83], nanostructured organic electrodes display interesting features that can address the redox mechanism-oriented issues and even trigger new mechanisms.

1. As discussed, irreversible structural phase transitions occur during the first sodiation of ketone-typed electrodes [65–68]. They cause large volume change and raise high stress/strain, often resulting in a large amount of defects (cracks, dislocations, plastic deformations, among others) and increasing charge transfer resistance in the host materials. Nanostructures could facilitate to release the stress/strain and suppress pulverization, so the organic electrodes can remain intact over cycles. For instance, less cracks and morphological deformation were found in the nanostructured DSR (Fig. 17a) [66] and CADS [68]. DSR nanorods showed higher capacity and rate capability than the microrod and microbulk counterparts. The better kinetics of the nanorod electrode was attributed to the reduced interface resistance (100 X vs. 320 and 720 X) and higher Na-ion diffusion coefficient (7.9×10^{-16} cm^2 s^{-1} vs. 1.96×10^{-16} and 4.36×10^{-17} cm^2 s^{-1}).
2. Because of the nature of doping/de-doping mechanism, large surface area and thin thickness are imperative for CPs to reach high contact interfaces with electrolyte for easy electrolyte penetration. Nanostructured CPs with hollow and/or porous features could have increased surface area and decreased thickness, realizing more active sites and short ion diffusion and electron transport paths. For instance, 2D mesoporous PPy nanosheets have pore size of 6.8–13.6 nm, ultrathin thickness of 25–30 nm, and surface area up to 96 m^2 g^{-1} (Fig. 17b) [77]. They delivered capacities of 123 and 83 mAh g^{-1} at 50 and 300 mA g^{-1}, respectively, which

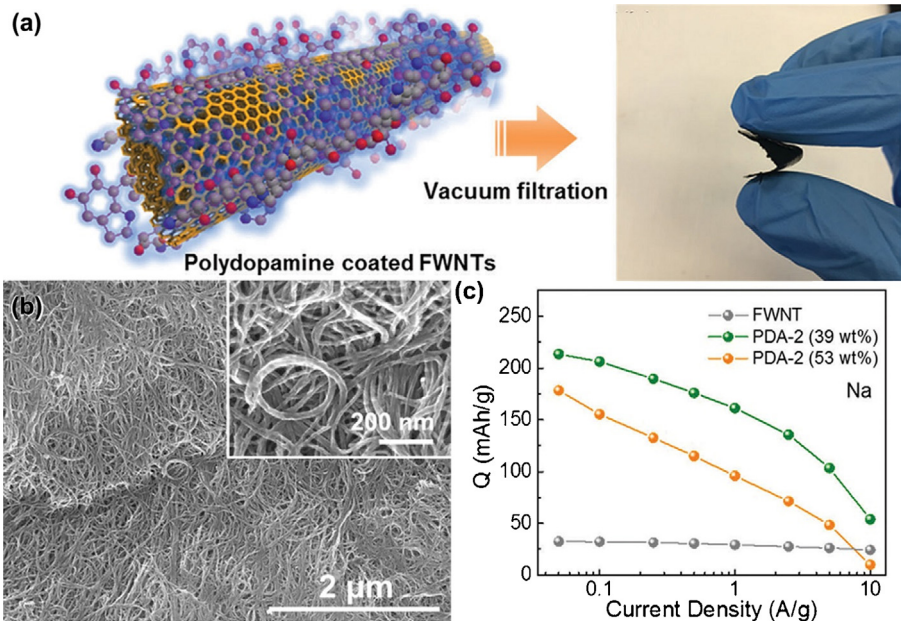

FIG. 18

(a) Illustration of the PDA coated-CNTs and the digital image of the flexible hybrid film. SEM image (b, inset: SEM image with high-magnification) and discharge capacities at different rate of the PDA coated-CNTs electrode (c). Reproduced with permission [86]. Copyright 2016, Royal Society of Chemistry.

were nearly twice more than irregular particles. Great rate capability was achieved in submicron PPy particles that kept a capacity of 84 mAh g^{-1} after 500 cycles at a high rate of 14.4 A g^{-1} [78].

3. Enhancement of electrochemical performance enabled by nanostructured organic compounds can be attributed to not only size effect but also new mechanisms that cannot be disclosed in bulk materials. In bulk Na_2TP, the desodiation proceeded by two one-electron transfers through an intermediate radical anion. By contrast, a new one-step desodiation process with two-electron transfer was observed in Na_2TP nanosheets (Fig. 17c and d) [107]. As a result, the nanosheet electrode exhibited much improved electrochemical properties in terms of larger capacity (248 vs. 199 mAh g^{-1}), higher rate capability (1.55 times more capacity at 1.25 A g^{-1}), and better cycle life (105 vs. 60 mAh g^{-1} after 100 cycles at 250 mA g^{-1}). Such improvement could be possibly ascribed to the new desodization mechanism and the optimized ionic/electronic transfer pathways in the nanosheet system.

Composites with carbon materials

Both small molecules and polymers have been incorporated with carbon materials to form composite electrodes in OSIBs. The carbon materials so far include carbon nanofibers [87], CNTs [58,86,95], graphene [38,108], GO [68], rGO [63,83], and mesoporous carbon [62]. They enable fast electron transport within the electrode matrix and could form strong interactions with the organic compounds. Therefore, composites with carbon materials offer the possibility to increase electronic conductivity and reduce solubility simultaneously.

Uniform mixing of the two components is crucial to achieve better electrochemical performances, for which solution-mixing method followed by a drying process is preferred, especially for small molecules of soluble sodium salts. A Na_2BDQ/CNTs anode prepared by spray drying exhibited a capacity of 259 mAh g^{-1} with an ICE of 88% and maintained 55% of the capacity at ~2 A g^{-1} [58]. Na_2TP/graphene composite synthesized via freeze-drying technique displayed an interconnected, multi-channeled monolith structure that promoted to achieve high capacity (268.9 mAh g^{-1}) and prolonged cyclability (77% retention after 500 cycles) [108]. It is worth pointing out that the solution-mixing method mostly results in a physisorption between the organic molecules and carbon materials, thus a certain amount of conductive additive (15–40 wt%) is still needed to ensure high electronic conductivity.

Strong interaction between the two components is another crucial factor because it can significantly reduce the dissolution of organic compounds, thereby increasing the utilization of their redox activities. It also can ensure high electronic conductivity and potentially eliminate the use of conductive additive and/or binder, resulting in higher energy density and flexible electrodes. One approach to strength the interaction is to synthesize organic compounds in situ. PDA-coated CNTs were synthesized by in situ polymerizing dopamine in a suspension of CNTs [86]. Continuous vacuum filtration of the hybrid produced a free-standing film that was used as a conductive additive- and binder-free electrode (Fig. 18a and b). Reversible capacities of 213 mAh g^{-1} at 50 mA g^{-1} and 54 mAh g^{-1} at 10 A g^{-1} were obtained due to the minimum dissolution of PDA ensured by the strong interactions at the PDA/CNTs interface and the porous network of the CNTs (Fig. 18c). Another approach is to use the π–π stacking interactions between small molecules with extended aromatic systems and carbon materials. A Juglone/rGO composite electrode was prepared by directly immersing Cu foil into a solution containing both components where Juglone was immobilized onto rGO nanosheets owing to the strong π–π interaction [63]. The electrode maintained high capacities of 280 and 212 mAh g^{-1} after 100 and 300 cycles, respectively, and displayed flexibility even in a big size 900 cm^2.

Encapsulation of organic molecules into mesoporous carbon materials provides another way to largely reduce the dissolution. For instance, CMK-3 with a large surface area, ordered porous

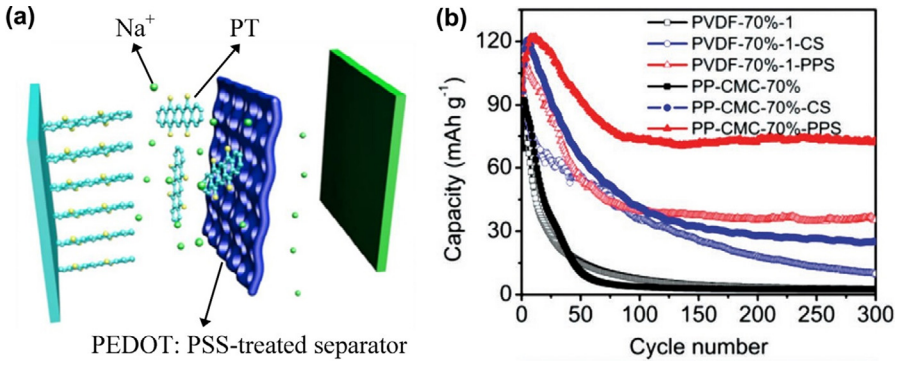

FIG. 19

(a) Illustration of the function of the PEDOT:PSS-treated separator. (b) Cycling performance of the PT electrodes. Reproduced with permission [111]. Copyright 2016, Wiley-VCH.

network, and good electronic conductivity was used to encapsulate AQ in its nanochannels [62]. The composite displayed an enhanced capacity of 214 mAh g^{-1} and 88% retention over 50 cycles over pure AQ (178 mAh g^{-1} and 71%). Radical polymer PTMA was successfully encapsulated in CNTs with a diameter of ~90 nm [95]. No self-discharge was observed from the composite, indicating a much reduced dissolution of PTMA.

Strategies to reduce the solubility of OSIB electrode materials

Dissolving in organic electrolyte perhaps is the most challenging issue when applying organic materials in OSIBs, which makes it worthy to summarize the available strategies to solve this issue in a separate section. Some strategies have been discussed throughout the two previous sections. They are either related to the molecules themselves, such as forming large π-conjugated system [37,45,54], forming organic salts [41,70], and polymerization [46,48,59,88], or related to electrode configurations, such as thin-film coating [31,55] and immobilization on conductive substrates [62,86,95]. As important as these strategies, those related to electrolyte and separator were equally effective but have received less attention. In this section, we will present recent investigations on electrolyte and separator in OSIBs.

The role of electrolyte is perhaps even more important in OSIBs than in inorganic SIBs as organic electrode materials are more or less soluble in electrolyte [39,55,62]. Mihali *et al.* tested a series of electrolytes with different compositions of sodium salts and solvents and found that battery performance was less dependent on the solvents, but rather on the sodium salts [39]. Electrolyte using sodium bis(fluorosulfonyl)imide (NaFSI) delivered better capacity retention than those using $NaClO_4$ and $NaPF_6$ regardless of the solvents. Along this line, Guo *et al.* proved that concentration of the sodium salts could also be crucial [62]. In an ether-based electrolyte, enhanced cyclability and rate capability were achieved with a high concentration (4 M) of CF_3SO_3Na (NaTFS) comparing with low concentrations (1–3 M). The enhancement can be ascribed to two reasons: (1) high concentration of sodium salts almost saturates the solvent, so the active material becomes hardly soluble; (2) high concentration of sodium salts produces more unsolvated Na-ions that have higher mobility. Considering that electrolytes with high concentration of salts seem beneficial in other ion-battery systems [109,110], this strategy might worth more in-depth studies in OSIBs.

Functionalization of separators for reducing solubility could potentially save tedious modification on the materials, reduce the cost of fabrication, and moreover, hold the advantage of generality to different active materials. For this purpose, Wang *et al.* proposed a selectively permeable membrane as separator in OSIBs [111]. The membrane was obtained by coating a layer of poly(3,4-ethylenedioxythiophene)-poly(styrene sulfonate) (PEDOT:PSS) onto glass fiber using a facile drop-casting method. It allows Na-ions to diffuse through but blocks the dissolved organic molecules owing to the high Na-ion conductivity and pinhole-free feature of PEDOT:PSS (Fig. 19a). The increased concentration of the molecules in the solvent can inhibit further dissolution. When applied this membrane to a highly soluble material 5,7,12,14-pentacenetetrone (PT), the capacity retention over 300 cycles were enhanced by at least two magnitudes (Fig. 19b). The generality of the membrane was demonstrated using another material DSR. It needs to point out that the initial dissolution of the organic materials was inevitable; nevertheless, the simplicity, effectiveness, and generality of this strategy contribute to the promise on long-term cycling stability.

Using above strategies should be closely referring to the characteristics of the used organic materials, for which one strategy may deliver better results than another. All the strategies can essentially reduce the solubility of the materials but it is difficult to completely avoid dissolution with liquid electrolytes being involved. A solid state electrolyte could completely prevent the materials from dissolving, but might lead to low ion conductivity at room temperature and large resistance at solid/solid interface. So far there has been no report regarding solid state electrolytes in OSIBs.

Comparison between OSIBs and OLIBs

SIBs and LIBs share similar working principle but exhibit different electrochemical performance even if same material is used, for which the larger size of Na-ion over Li-ion (1.02 Å vs. 0.76 Å) is generally believed to be responsible. Inorganic electrode materials receive complex requirements on their rigid crystal structures to cope with the large sized Na-ions, thus it is not

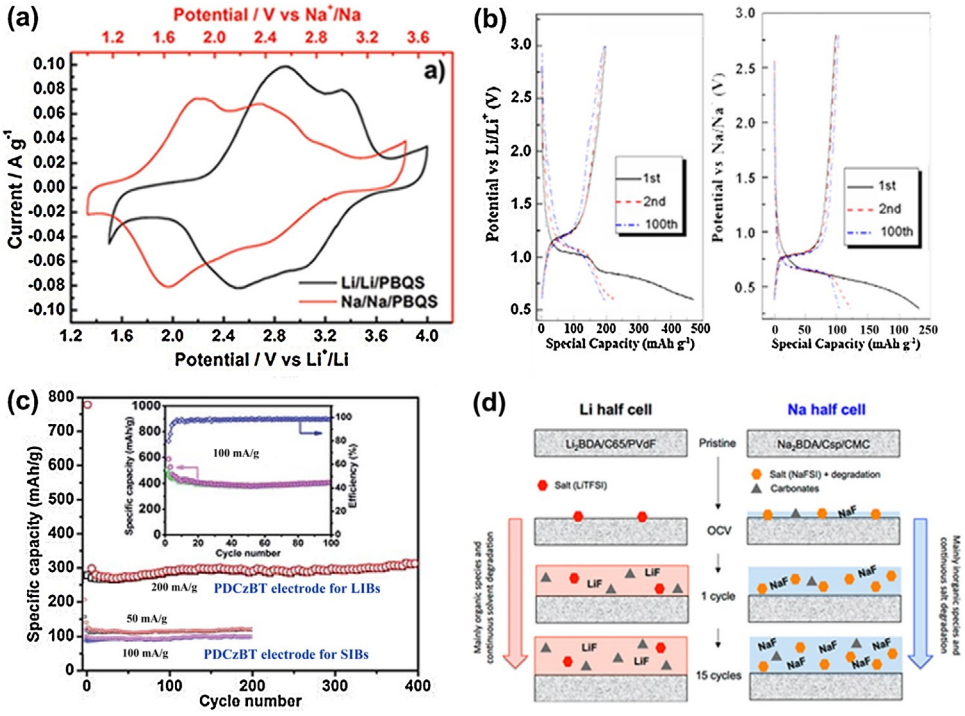

FIG. 20

(a) CV curves of the Li/Li/PBQS and Na/Na/PBQS batteries at 0.1 mV s^{-1}. Reproduced with permission [60]. Copyright 2015, Wiley-VCH. (b) Charge–discharge curves of LiPTCDA and NaPTCDA at 25 mA g^{-1}. Reproduced with permission [35]. Copyright 2013, Elsevier. (c) Cycling performance of the PDCzBT electrode in LIBs and SIBs. Reproduced with permission [90]. Copyright 2015, Royal Society of Chemistry. (d) Schematic evolution of the electrode–electrolyte interface layer on the Li_2BDA and Na_2BDA electrodes in the Li- and Na-half cell, respectively. Reproduced with permission [40]. Copyright 2016, American Chemical Society.

feasible to simply transplant the materials from LIBs to SIBs. By contrast, organic electrode materials have flexible molecular structures and can accommodate Na-ions reversibly without much spatial hindrance, making it feasible to simply transplant metal-free organic materials from LIBs to SIBs or, in some cases, lithium salts to sodium salts. However, the transplant of materials does not guarantee a transplant of performances. Discrepancy of performances is related to processes occurring both within the solid materials and on the solid material/liquid electrolyte interface during the electrochemical reaction.

On one hand, the larger size of Na-ion can induce larger energy barrier to overcome, resulting in a reduced redox potential. In the three-electrode batteries of Na/Na/PBQS and Li/Li/PBQS, despite that the similarity of the CV curves verified the same redox reaction mechanism with either Na^+ or Li^+, a largely reduced potential was found in the Na system [60]. After eliminating the anode polarization and deducting the standard potential gap between Na/Na^+ and Li/Li^+ couple (0.33 V), an absolute redox potential of PBQS in the Na system still negatively shifted by ~0.3 V (Fig. 20a). In addition to quinones, the negative shift of redox potential can be found in other Na/Li homologues such as Na_2TP/Li_2TP [27,31,32] and NaPTCDA/LiPTCDA [35,36]. Larger Na-ions also can display poorer kinetics when bonding with or dissociating from aromatic cores, causing a lowered utilization of the functional groups and decreased capacity. NaPTCDA exhibited a capacity roughly half as much as LiPTCDA (Fig. 20b), indicating a two-electron transfer in the Na system instead of a four-electron transfer in the Li system even though there are four carbonyl groups in both molecules [35,36]. When polymers were applied in OSIBs, the more sluggish kinetics can cause a lower doping and absorbing amount of Na-ions. For instance, PDCzBT delivered a significantly less capacity doping with Na^+ than with Li^+ (Fig. 20c) [90].

On the other hand, a large irreversible capacity is often experienced in both OSIBs and OLIBs, and generally contributes to SEI layer that could be decisive for battery performance. The SEI layer and its evolution can be very different in the Na and Li systems even with Na/Li homologues as electrodes. Taking Na_2BDA and Li_2BDA as examples (Fig. 20d) [39,40], the

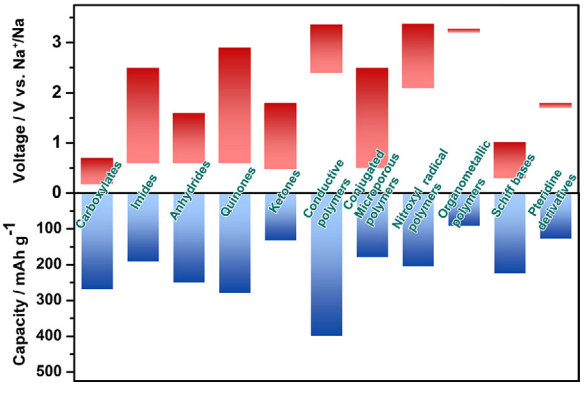

FIG. 21

Overview of the discharge potential and capacity of the reported organic electrode materials.

Na-based electrode reacted spontaneously with the electrolyte and the SEI layer was dominated by inorganic species with continuous salt degradation during cycling. Differently, the Li-based electrode displayed an SEI layer with primarily organic species from the solvent degradation products appearing only after cycling and increasing in amount with prolonging cycles. These results undoubtedly suggest that more studies on SEI layer are highly desirable; given the consideration that SEI layer is a major source of aging of anode materials.

Future challenges and opportunities

The development of renewable and environmentally responsible organic sodium-ion batteries has gained remarkably increased attentions in the past six years. Much effort in this field has accumulated rich knowledges and greatly pushed forward the performances of OSIBs (Fig. 21). Our review provides a systematical summary of OSIBs by presenting the recent progress in the perspectives of molecular design and electrode design. Solutions to reduce the solubility of organic materials are given special attentions and the crucial differences between OLIBs and OSIBs are also included aiming to spark future rational designs. Our goal is to reveal the key issues, possibilities and opportunities at present and in future. Although great achievements have been made in advancing OSIBs, many challenges still remain in the areas of chemistry, material science and engineering.

At present, despite that it is difficult to find satisfactory organic electrode materials after balancing complex requirements of SIBs, simulations have shown great potential as a powerful tool for exploring new reversible active reaction groups and reaction mechanisms of battery electrodes. As for the conventional organic materials, simulations can also contribute to the solutions toward the existing problems of active groups, or predicting new materials by the combination of various active groups. Guided by simulations, the developing synthetic route together with advanced characterization tools would realize more rational designs of active organic molecules with high performance and offer more possibilities for deep insights of electrochemical steps, offering new routes of molecule simulations.

Organic electrode materials in SIBs behave inherent fast reaction kinetics and easy control on functional groups, allowing promising applications of organic materials in other electrochemical energy storage systems with high energy and power density. Conductive polymers, nitroxyl radical polymers and conjugated carbonyl compounds have been employed as electrode candidates for pseudocapacitors [112,113]. Very recently, K_2TP [114,115] and PTCDA [116] were demonstrated as a suitable anode material in potassium-ion batteries, indicating a possible extension of organic materials to the rechargeable battery systems beyond Li and Na (Mg, Al, Li-S, among others). As discussed in this review, the solubility issue is the main obstacle to apply organic materials in SIBs, however, it promotes the electrochemical reactions occurring in solution phases. For instance, great solubility and structural diversity of organic materials can enable broad space to explore their applications in redox flow batteries [117].

With recent advances in portable electronics and roll-up displays, there is a tendency of rendering batteries thinner, smaller, flexible and wearable. Compared with fragile inorganic materials, organic materials show superiorities including the characteristics of solubility, film-forming ability, and sublimability. It is therefore facile to load organic materials onto flexible current collectors by casting, printing, vapor deposition, vacuum filtration and in situ polymerization, among others, promoting the realization of flexible devices. Furthermore, organic materials also enable the contributions on the binders, current collectors and separators in the flexible batteries. Developing suitable organic materials for each unit exhibits bright prospects.

Researchers have attempted to utilize organic electrode materials in aqueous SIBs because aqueous electrolytes possess several advantages over organic electrolytes, such as non-flammability, low price, less strict battery assembling conditions, and high ionic conductivity. Use of aqueous electrolytes requires appropriate organic materials that operate within the electrochemically stable window of water, meaning that the electrode redox potentials should be located between those of H_2 and O_2 evolution (2.297 and 3.527 V vs. Na/Na^+ at pH = 7 without overpotentials) [118]. It results in limited choices of polymeric electrode materials in aqueous SIBs (Fig. 21) and they are mainly applied to anodes due to their redox potentials and the absence of Na-ions in pristine states. NTCDA-derived polyimides [119–123] with the redox potentials of 2.2–2.4 V are the only type reported so far. The redox mechanism is same as in the organic electrolytes and the delivered capacities are comparable (140–160 mAh g^{-1}). The polyimides generally exhibited favorable cyclability and rate capability up to 2 A g^{-1} as the result of (i) the Na-storage mechanism involves minimum volumetric change of the host structures, (ii) the flexible polymer framework is mechanically robust against Na-insertion, and (iii) the high chemical resistivity of the polymers reduces their dissolution in the electrolytes [118]. Besides, symmetric cells using PPy as both electrodes showed a capacity over 100 mAh g^{-1} [124]. A nitroxyl radical polymer poly(2,2,6,6-tetra-methylpiperidinyloxy-4-yl viylether) (PTVE) with a redox potential of ~3.6 V (vs. Na/Na^+) was examined in aqueous electrolytes but the one-electron oxidation of it to the oxoammonium cation salt does not involve Na-ions [125,126]. In addition, biologically derived melanin [127] and metal-organic frameworks [128] were reported but displayed very limited long-term cycling capacities. The application of aqueous OSIBs is still in its infancy and facing several challenges. First, sodium-containing inorganic cathodes are needed to compensate for the absence of sodium in the anodes and the associated low redox potentials. Second, the narrow stable window of aqueous electrolytes (~2.0 V expanded by the kinetic effects during electrolysis) leads to a much lower energy density (<40 Wh kg^{-1}) than that in organic electrolytes. Third, the operating potential and pH value of the aqueous electrolytes needs to be wisely chosen to avoid H_2/O_2 evolution reaction which would affect the stability of the electrode materials. Last but not least, the dissolved O_2 in the electrolytes needs to be eliminated because it could decrease the stability of the electrode materials by oxidizing the sodiated electrode materials [129].

Acknowledgements

This work was supported by the European Research Council (ThreeDsurface, 240144, and HiNaPc, 737616), BMBF (ZIK-

3DNanoDevice, 03Z1MN11), and German Research Foundation (DFG: LE 2249_4-1). We thank Prof. Zhi Li for the helpful discussions with him.

References

[1] D. Kundu et al., Angew. Chem. Int. Ed. 54 (2015) 3431.
[2] J.-M. Tarascon, Nat. Chem. 2 (2010) 510.
[3] M.S. Whittingham, Prog. Solid State Chem. 12 (1978) 41.
[4] A.S. Nagelberg, W.L. Worrell, J. Solid State Chem. 29 (1979) 345.
[5] C. Delmas et al., Solid State Ion. 3 (1981) 165.
[6] K. Abraham, Solid State Ion. 7 (1982) 199.
[7] T. Jow et al., J. Electrochem. Soc. 134 (1987) 1730.
[8] N. Yabuuchi et al., Chem. Rev. 114 (2014) 11636.
[9] Y. Xu et al., Adv. Energy Mater. 6 (2016) 1502514.
[10] E.M. Lotfabad et al., ACS Nano 8 (2014) 7115.
[11] Y. Xu et al., Angew. Chem. Int. Ed. 54 (2015) 8768.
[12] M. Zhou et al., Adv. Energy Mater. 6 (2016) 1600448.
[13] J. Sun et al., Nat. Nanotechnol. 10 (2015) 980.
[14] L. Liang et al., Energy Environ. Sci. 8 (2015) 2954.
[15] Y. Wen et al., Nat. Commun. 5 (2014).
[16] P. Barpanda et al., Nat. Commun. 5 (2014).
[17] N. Yabuuchi et al., Nat. Mater. 11 (2012) 512.
[18] M. Zhou et al., Nano Energy 31 (2017) 514.
[19] P. Poizot, F. Dolhem, Energy Environ. Sci. 4 (2011) 2003.
[20] Y. Liang et al., Adv. Energy Mater. 2 (2012) 742.
[21] Z. Song, H. Zhou, Energy Environ. Sci. 6 (2013) 2280.
[22] B. Häupler et al., Adv. Energy Mater. 5 (2015) 1402034.
[23] V.A. Oltean et al., Materials 9 (2016) 142.
[24] H. Pan et al., Energy Environ. Sci. 6 (2013) 2338.
[25] V. Palomares et al., Energy Environ. Sci. 5 (2012) 5884.
[26] J. Geng et al., Energy Environ. Sci. 3 (2010) 1929.
[27] M. Armand et al., Nat. Mater. 8 (2009) 120.
[28] Z. Song et al., Angew. Chem. 122 (2010) 8622.
[29] B. Genorio et al., Angew. Chem. Int. Ed. 49 (2010) 7222.
[30] H. Chen et al., ChemSusChem 1 (2008) 348.
[31] L. Zhao et al., Adv. Energy Mater. 2 (2012) 962.
[32] Y. Park et al., Adv. Mater. 24 (2012) 3562.
[33] A. Abouimrane et al., Energy Environ. Sci. 5 (2012) 9632.
[34] A. Choi et al., J. Mater. Chem. A 2 (2014) 14986.
[35] R. Zhao et al., J. Electroanal. Chem. 688 (2013) 93.
[36] M. Veerababu et al., Int. J. Hydrogen Energy 40 (2015) 14925.
[37] C. Wang et al., J. Am. Chem. Soc. 137 (2015) 3124.
[38] W. Deng et al., Small 12 (2016) 583.
[39] V.A. Mihali et al., RSC Adv. 4 (2014) 38004.
[40] V.A. Oltean et al., Chem. Mater. 28 (2016) 8742.
[41] Y. Zhang et al., Chem. Commun. 52 (2016) 9969.
[42] J. Xue et al., Electrochim. Acta 219 (2016) 418.
[43] S. Wang et al., Angew. Chem. Int. Ed. 53 (2014) 5892.
[44] S. Renault et al., Electrochem. Commun. 45 (2014) 52.
[45] W. Deng et al., ACS Appl. Mater. Interfaces 7 (2015) 21095.
[46] H.G. Wang et al., Adv. Energy Mater. 4 (2014) 1301651.
[47] F. Xu et al., Electrochem. Commun. 60 (2015) 117.
[48] F. Xu et al., J. Mater. Chem. A 4 (2016) 11491.
[49] L. Chen et al., RSC Adv. 4 (2014) 25369.
[50] F. Xu et al., Mater. Chem. Phys. 169 (2016) 192.
[51] H. Banda et al., J. Mater. Chem. A 3 (2015) 10453.
[52] Z. Li et al., Chem. Eng. J. 287 (2016) 516.
[53] W. Luo et al., Adv. Energy Mater. 4 (2014).
[54] H.-g. Wang et al., Energy Environ. Sci. 8 (2015) 3160.
[55] C. Luo et al., Nano Energy 13 (2015) 537.
[56] Z. Zhu et al., Chem. Commun. 51 (2015) 1446.
[57] X. Wu et al., Sci. Adv. 1 (2015) e1500330.
[58] X. Wu et al., J. Mater. Chem. A 3 (2015) 13193.
[59] W. Deng et al., Sci. Rep. 3 (2013) 2671.
[60] Z. Song et al., Adv. Sci. 2 (2015) 1500124.
[61] D. Wu et al., Chem. Commun. 52 (2016) 11207.
[62] C. Guo et al., Chem. Commun. 51 (2015) 10244.
[63] H. Wang et al., Adv. Mater. 27 (2015) 2348.
[64] H. Kim et al., Chem. Mater. 27 (2015) 7258.
[65] K. Chihara et al., Electrochim. Acta 110 (2013) 240.
[66] Y. Wang et al., Nano Lett. 16 (2016) 3329.
[67] C. Wang et al., Adv. Funct. Mater. 26 (2016) 1777.
[68] C. Luo et al., J. Power Sources 250 (2014) 372.
[69] S. Wu et al., Nat. Commun. 7 (2016).
[70] M. Yao et al., Sci. Rep. 4 (2014) 3650.
[71] H. Zhu et al., Chem. Commun. 51 (2015) 14708.
[72] L. Shacklette et al., J. Electrochem. Soc. 132 (1985) 1529.
[73] M. Zhou et al., RSC Adv. 2 (2012) 5495.
[74] L. Zhu et al., Chem. Commun. 49 (2013) 11370.
[75] M. Zhou et al., J. Polym. Sci. Polym. Phys. 51 (2013) 114.
[76] D. Su et al., Chem. Commun. 51 (2015) 16092.
[77] S. Liu et al., Adv. Mater. 28 (2016) 8365.
[78] X. Chen et al., RSC Adv. 6 (2016) 2345.
[79] M. Zhou et al., Chem. Commun. 51 (2015) 14354.
[80] Y. Shen et al., Electrochem. Commun. 49 (2014) 5.
[81] R. Zhao et al., Electrochem. Commun. 21 (2012) 36.
[82] X. Zhu et al., Electrochim. Acta 178 (2015) 55.
[83] J. Chen et al., J. Mater. Sci. 50 (2015) 5466.
[84] S.C. Han et al., J. Power Sources 254 (2014) 73.
[85] T. Sun et al., Angew. Chem. 128 (2016) 10820.
[86] T. Liu et al., Energy Environ. Sci. 10 (2017) 205.
[87] L. Zhu et al., Electrochim. Acta 78 (2012) 27.
[88] K. Sakaushi et al., Nat. Commun. 4 (2013) 1485.
[89] K. Sakaushi et al., J. Power Sources 245 (2014) 553.
[90] S. Zhang et al., J. Mater. Chem. A 3 (2015) 1896.
[91] W. Guo et al., Energy Environ. Sci. 5 (2012) 5221.
[92] Q. Huang et al., Phys. Chem. Chem. Phys. 15 (2013) 20921.
[93] K. Nakahara et al., Chem. Phys. Lett. 359 (2002) 351.
[94] Y. Dai et al., Electrochem. Soc. 13 (2010) A22.
[95] J.-K. Kim et al., Energy Environ. Sci. 9 (2016) 1264.
[96] H. Zhong et al., Chem. Commun. 50 (2014) 6768.
[97] E. Castillo-Martínez et al., Angew. Chem. Int. Ed. 53 (2014) 5341.
[98] M. López-Herraiz et al., Energy Environ. Sci. 8 (2015) 3233.
[99] J. Hong et al., Nat. Commun. 5 (2014) 5335.
[100] R. Precht et al., Phys. Chem. Chem. Phys. 18 (2016) 3056.
[101] Y. Chen, S. Manzhos, Mater. Chem. Phys. 156 (2015) 180.
[102] Y. Chen, S. Manzhos, Phys. Chem. Chem. Phys. 18 (2016) 8874.
[103] C. Luo et al., Nano Lett. 14 (2014) 1596.
[104] M. Lee et al., Adv. Mater. 26 (2014) 2558.
[105] S. Wang et al., Nano Lett. 13 (2013) 4404.
[106] J.-K. Kim et al., J. Mater. Chem. A 1 (2013) 2426.
[107] F. Wan et al., Nano Energy 13 (2015) 450.
[108] Y. Wang et al., RSC Adv. 6 (2016) 57098.
[109] L. Suo et al., Nat. Commun. 4 (2013) 1481.
[110] M. He et al., Angew. Chem. 128 (2016) 15536.
[111] C. Wang et al., Adv. Mater. 28 (2016) 9182.
[112] H.-P. Cong et al., Energy Environ. Sci. 6 (2013) 1185.
[113] R.V. Salvatierra et al., Chem. Mater. 22 (2010) 5222.
[114] K. Lei et al., Energy Environ. Sci. 10 (2017) 552.
[115] Q. Deng et al., Nano Energy 33 (2017) 350.
[116] Y. Chen et al., Nano Energy 18 (2015) 205.
[117] W. Wang et al., Adv. Funct. Mater. 23 (2013) 970.
[118] H. Kim et al., Chem. Rev. 114 (2014) 11788.
[119] H. Qin et al., J. Power Sources 249 (2014) 367.
[120] W. Deng et al., Chem. Commun. 51 (2015) 5097.
[121] X. Dong et al., Sci. Adv. 2 (2016) e1501038.
[122] T. Gu et al., RSC Adv. 6 (2016) 53319.
[123] D. Kim et al., Adv. Energy Mater. 4 (2014) 1400133.
[124] Y. Wei et al., Org. Electron. 46 (2017) 211.
[125] K. Koshika et al., Chem. Commun. (2009) 836.
[126] K. Koshika et al., Macromol. Chem. Phys. 210 (2009) 1989.
[127] Y. Kim et al., Proc. Natl. Acad. Sci. U. S. A. 110 (2013) 20912.
[128] J. Chavez et al., RSC Adv. 7 (2017) 24312.
[129] Y. Wang et al., Adv. Energy Mater. 2 (2012) 830.